AN EXPERIMENTAL INVESTIGATION OF THE PARITY PURITY OF THE 110-keV GAMMA-DECAY OF ^{19}F

Thesis by

Robert Alan Moline

In Partial Fulfillment of the Requirements

For the Degree of

Doctor of Philosophy

California Institute of Technology

Pasadena, California

1969

(Submitted September 9, 1968)

ACKNOWLEDGMENTS

Thanks are due to Dr. Robert Stokstad, Dr. Anthony Adams, Dr. John Morris, Dr. Ernesto Maqueda, Professor Felix Boehm, and Dr. Aage Winther whose help and discussions at crucial periods during this experiment were most useful.

Special thanks are due Professor Charles Barnes whose guidance and encouragement were most appreciated, and I wish to thank him for suggesting the experiment to me and generating my interest in the problem.

Financial assistance was granted by the National Science Foundation and the California Institute of Technology and is gratefully acknowledged.

Thanks are also due the entire staff and personnel of the Kellogg Radiation Laboratory for their help and cooperation in the completion of this experiment.

ABSTRACT

If either, or both, of the ground state ($J^{\pi} = \frac{1}{2}^{+}$) and first excited state (110 keV, $J^{\pi} = \frac{1}{2}^{-}$) of the ^{19}F nucleus has impure parity, it follows that the de-excitation γ rays would have an angular distribution of the form,

$$W(\theta) = 1 + P\eta \cos(\theta) \ .$$

In this expression, θ is the angle between the chosen quantization axis and the photon momentum, and P is the polarization of the excited nuclei, with respect to the chosen quantization axis. By assuming the existence of a parity-violating, weak-interaction, nucleon-nucleon force, Maqueda has predicted that the asymmetry parameter, $|\eta|$ in the above expression, should be 4.3×10^{-4}.

The present experiment used the Coulomb excitation of 37.5-MeV ^{19}F projectiles in a gold target to produce $^{19}F^{*}$ (110 keV) nuclei with a large polarization perpendicular to the scattering plane. After being scattered in the gold foil, the $^{19}F^{*}$ nuclei recoiled into an iron cylinder. In the geometry used, there was essentially azimuthal symmetry, and therefore no net polarization on any axis perpendicular to the beam direction, until the iron stopper was magnetized. The magnetization produced a net polarization of the $^{19}F^{*}$ nuclei on a chosen axis perpendicular to the incident beam, by precessing the $^{19}F^{*}$ nuclei in the hyperfine field in the iron.

From the asymmetry observed in the γ-ray counting rate when the magnetization was reversed, the quantity $P\eta$ was determined to be $(6.6 \pm 5.9) \times 10^{-5}$.

Since the magnitude (and sign) of P is dependent on the hyperfine magnetic field, investigations were carried out to determine the average hyperfine field of fluorine in iron by using the nuclear reaction $^{16}O(^{3}He,p)^{18}F^{*}$ (937 keV).

A p-γ coincidence technique was used, and the average precession angle of the excited nuclei during their mean life of (68 ± 7) ps was observed, when the $^{18}F^{*}$ recoiled into an iron host lattice. The results indicate an average hyperfine field of (88 ± 19) kG for fluorine in iron, if the g-factor of the 937-keV state is assumed to have the theoretical value 0.61.

There was evidence of serious radiation damage in the iron, produced by the ^{3}He beam and by recoils from the target, during some of the magnetic field measurements. To investigate this effect, a thin iron foil was bombarded with a 100-keV ^{19}F beam. At a radiation dosage of between 2×10^{16} and 7×10^{16} fluorine ions per cm^2 the permeability of the iron changed dramatically, in such a way that a several times stronger external field was required to saturate the iron.

If it is assumed that the 110-keV level of ^{19}F has a g-factor of -0.57 and a mean life of 0.88 ns, the most probable value for the net polarization is 0.109 ± 0.023, resulting in an asymmetry coefficient, η, of $(6.1 \pm 5.6) \times 10^{-4}$.

TABLE OF CONTENTS

I. INTRODUCTION

Considerable effort has been directed toward the observations of weak, parity-violating interactions between nucleons. The first attempts looked for reactions which are absolutely forbidden if parity and angular momentum are conserved. Some examples of these reactions are; $^{20}Ne^{*}$ (13.19 MeV, $J^{\pi} = 1^{+}$) $\rightarrow$ $^{16}O + {}^{4}He$ (Tanner, 1957), $^{4}He + d \rightarrow {}^{6}Li^{*}$ (3.56 MeV, $J^{\pi} = 0^{+}$) (Wilkinson, 1958), and $^{16}O^{*}$ (8.88 MeV, $J^{\pi} = 2^{-}$) $\rightarrow$ $^{12}C + {}^{4}He$ (Segel et al., 1961). These experiments are sensitive to the square of the amplitude of the parity admixture in the wave function.

Other experiments reported in the literature have used heavy nuclei as a source of γ radiation and have searched for interference effects between γ-decays of mixed multipolarity which imply that the nuclear energy levels are not of a pure parity (assuming that the electromagnetic interaction conserves parity). These experiments are sensitive to the amplitude of the parity admixture, as distinct from the amplitude squared. Some of these results have recently been summarized by McKellar (1968).

In one type of experiment, a net γ-ray circular polarization is measured for decays from an unpolarized radioactive source. This has been done for ^{175}Lu, ^{181}Ta, ^{203}Tl, and ^{180m}Hf (Boehm and Kankeleit, 1968; Lobashov et al., 1967; Paul et al., 1967). The results of a different kind of experiment, a search for a $\cos(\theta)$ term in the γ-decay of $^{114}Cd^{*}$ following polarized-neutron capture,

have been published by a number of authors and most recently by Abov et al. (1968).

This thesis describes a search for a $\cos(\theta)$ term in the angular distribution of the γ-decay of polarized $^{19}F^*$ (110 keV, $J^\pi = \frac{1}{2}^-$), where θ is the angle between the $^{19}F^*$ polarization and the momentum of the photons. The present experiment has the potential advantage that, since the ^{19}F nucleus contains considerably fewer particles than the heavy nuclei examined previously, the nuclear physics of this nucleus is more nearly understood. Thus, more accurate theoretical predictions for the magnitude of the parity-violation effects should eventually be possible.

Part II of the thesis outlines the theory and calculations which lead to a rough prediction for the magnitude of the parity-violation in the $^{19}F^*$ γ-decay. Part III describes the experimental method, and Part IV gives the experimental results with the necessary corrections to yield a physically significant answer.

Part V discusses the hyperfine field at the site of a fluorine nucleus implanted in an iron host lattice. Since this magnetic field is crucial to the interpretation of the present experiment, a number of subsidiary experiments were carried out to clarify this poorly understood subject. Part VI discusses the significance of the effect and makes suggestions as to how the experiment might be improved in further studies.

II. THEORY OF PARITY NON-CONSERVING INTERACTIONS

In 1958 Gell-Mann and Feynman (Feynman and Gell-Mann, 1958) postulated that the interaction Lagrangian for the weak interaction is of the form

$$\mathcal{L} = \sqrt{8}\, G\, J_\mu\, J_\mu^+ ,$$

where G is the weak interaction coupling constant, and the current, J_μ, is written as

$$J_\mu = (\bar{e}\ \gamma_\mu a \nu_e) + (\bar{\mu}\ \gamma_\mu a \nu_\mu) + (\bar{n} \gamma_\mu a p) + \ldots ,$$

with

$$a = \tfrac{1}{2}\ (1 + i\gamma_5) .$$

This form of the interaction describes, in a very elegant way, β-decay, μ-decay, and the other known weak decays, both strangeness-conserving and strangeness-violating, but the existence of "self-terms" in the Lagrangian, of the form

$$(\bar{e}\gamma_\mu a \nu_e)\ (\bar{e}\gamma_\mu a \nu_e)^+ ,$$

has not yet been confirmed experimentally. This term, for example, would predict (e,ν_e) scattering, or, in crossed form, the reaction

$$e^+ + e^- \rightarrow \nu_e + \bar{\nu}_e ,$$

a reaction which would contribute significantly to the energy loss from stars having internal temperatures, $T \gtrsim 10^9\ ^oK$.

The self-terms of the form $(\bar{n}\gamma_\mu ap)\ (\bar{n}\gamma_\mu ap)^+$ predict interactions described by Feynman diagrams of the type

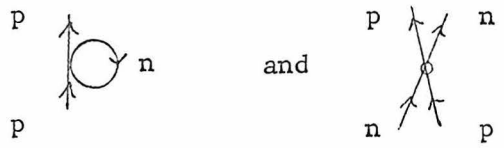

which would cause nuclear levels to have small, predictable admixtures of a parity opposite to the normal parity. Michel (1964) has considered the parity impurity of nuclear levels extensively, in a general way, and the expected asymmetry ($\cos(\theta)$ term) for the $J^\pi = \frac{1}{2}^- \rightarrow \frac{1}{2}^+$ transition of ^{19}F has been calculated by Maqueda (1966) using Michel's parity-violating potential.

Consider the ground state and the 110-keV level of ^{19}F as shown in Figure 1. If the levels are not assumed to have pure parity, the true wave function, ψ, can be written as a superposition of wave functions, χ, of pure parity.

Let the excited state wave function be

$$\psi(\tfrac{1}{2}^-) = \chi(\tfrac{1}{2}^-) + \frac{\epsilon}{\Delta E}\ \chi(\tfrac{1}{2}^+)\ ,$$

where we make the explicit assumption that the dominant parity mixing involves only these two states. ΔE is the energy difference $E(\frac{1}{2}^-) - E(\frac{1}{2}^+)$ and ϵ is proportional to the weak interaction coupling constant; the magnitude of ϵ is derived by using first-order

FIGURE 1

Level schemes of ^{19}F and ^{18}F. The ^{19}F data are taken from Lauritsen and Ajzenberg-Selove (1962) and the ^{18}F data are taken from Olness and Warburton (1967).

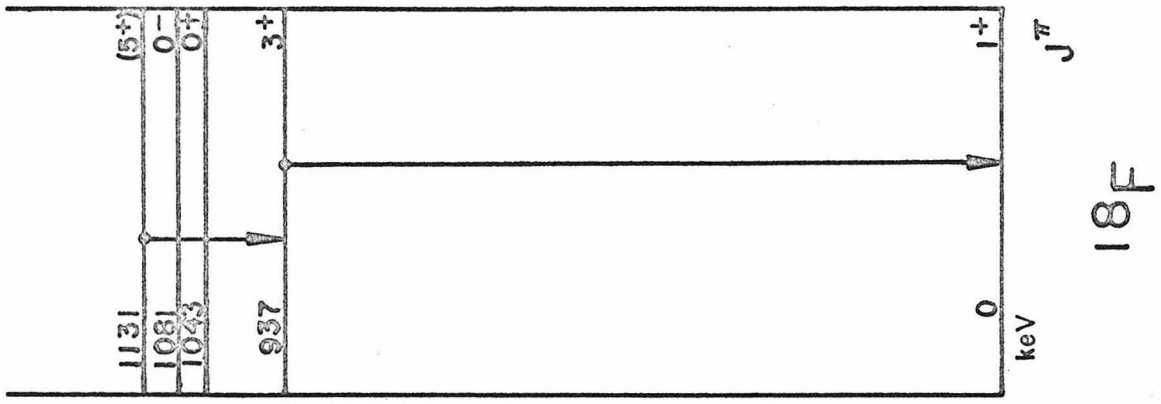
(5+)
0−
0+
3+
1+
Jπ
1131
1081
1043
937
0
keV
18F

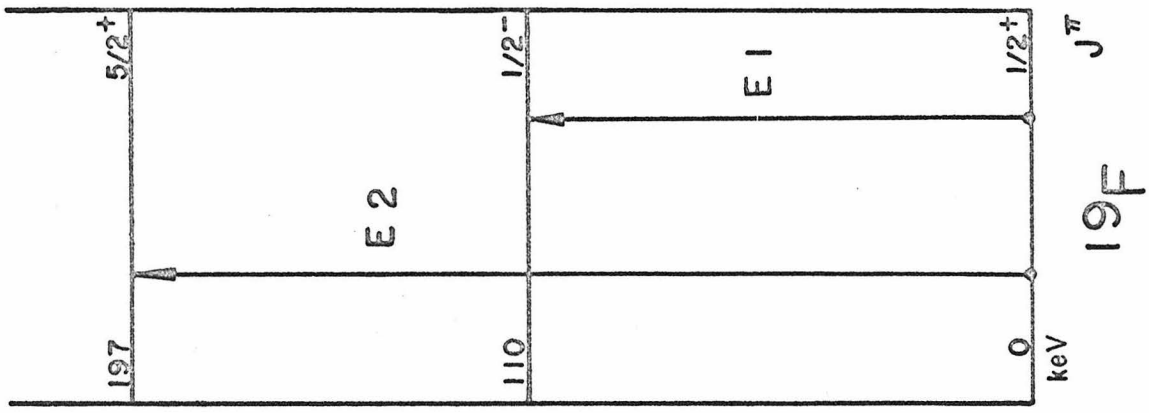
5/2+
1/2−
1/2+
Jπ
E2
E1
197
110
0
keV
19F

FIGURE 1

perturbation theory. With the above expression for $\psi(\frac{1}{2}^-)$, we have, for the ground state,

$$\psi(\tfrac{1}{2}^+) = \chi(\tfrac{1}{2}^+) - \frac{\epsilon^*}{\Delta E}\ \chi(\tfrac{1}{2}^-) \ .$$

The possible channels for γ-decay are:

(1) $\chi(\frac{1}{2}^-) \rightarrow \chi(\frac{1}{2}^+)$ which is 0^{th} order in ϵ (E1),

(2) $\chi(\frac{1}{2}^-) \rightarrow \chi(\frac{1}{2}^-)$ which is 1^{st} order in ϵ (M1),

(3) $\chi(\frac{1}{2}^+) \rightarrow \chi(\frac{1}{2}^+)$ which is 1^{st} order in ϵ (M1), and

(4) terms of order ϵ^2.

In the above expressions E1 (M1) denotes electric (magnetic) dipole γ-ray decay.

The E1 and M1 decay amplitudes mix, causing, in effect, a rotating dipole (the M1 amplitude is 90^o out of phase with the E1 amplitude). This rotating dipole would cause a net circular polarization of γ rays, even from an unpolarized source of $^{19}F^*$. It also yields an up-down asymmetry from polarized $^{19}F^*$ nuclei. An angular distribution of the form

$$W(\theta) = 1 + P\eta \cos(\theta)$$

is predicted, where

$$\cos(\theta) = \frac{\vec{z} \cdot \vec{k}}{|z|\ |k|} ,$$

$\vec{z}$ is the axis of quantization of the spin of the $^{19}F^*$ nuclei, $\vec{k}$ is the momentum vector of the photon, and P is the fractional polarization of the nuclei. The predicted value of $|\eta|$ is 4.3×10^{-4} (Maqueda, 1966).

This result was derived using a single-particle parity non-conserving potential of the form $v = F(\hbar/MR_o)\vec{\sigma} \cdot \vec{\rho}$ with a value of $F = 3.2 \times 10^{-7}$. η also depends linearly on the difference between the magnetic moments of the first excited state and the ground state. The measured magnetic moment of the ground state is 2.6287 n.m. The magnetic moment of the $\frac{1}{2}^-$ state has not been measured but it is expected to be $\approx$ -0.28 n.m. (Maqueda, 1966), an estimate which is based on the nuclear magnetic moment of the ground state of ^{15}N. Even if this estimate is somewhat in error, the difference of the two magnetic moments is not likely to be changed significantly.

III. EXPERIMENTAL METHOD

Two γ-ray detectors were positioned so that, when a positive average $^{19}F^*$ polarization (P) was directed toward one γ-detector, a negative polarization was directed toward the other detector. The coefficient of the $\cos(\theta_\gamma)$ term is proportional to P as discussed in Part II. With the momentum vector of the γ ray taken as the axis of quantization of the spin of the $^{19}F^*$ nuclei, θ_γ equals zero. Therefore the count rate expected should be proportional to $(1 + \eta P)$.

The sign of P was changed 76 times a minute using a magnetic field as described below. Four γ-yields, $N_{1,2}^{+,-}$, were obtained, where $N_{1,2}^{+,-}$ is the number of γ rays recorded for detector 1,2 during the time the magnetic field reversing relay was in the +,- position. The ratio (See Appendix 2)

$$Q_A = (N_1^+/N_1^-)/(N_2^+/N_2^-)$$

was taken and the experiment repeated with the basic sign of P reversed, so that, if P was positive for N_1^+ for experiment A, P would be negative for N_1^+ for experiment B. Q_B was defined in the same way as Q_A and the ratio Q_A/Q_B computed. Q_A/Q_B is equal to $1 + 8\delta$, where the measured quantity δ is related to η in Part IV.

A. Source of Polarized $^{19}F^*$ Nuclei

The ONR-CIT tandem accelerator was used to produce a 37.5-MeV ^{19}F beam with an intensity of approximately 1 μampere of

charge-5^{+} ^{19}F ions. Singly-charged negative ^{19}F ions were formed by charge-exchange of the positive ions from the duoplasmatron ion source, which was operated on a mixture of 50 percent CF_4 and 50 percent He as the source gas. Mixtures with 1 percent CF_4 and 10 percent CF_4 were tried in the ion-source but neither gave sufficient ^{19}F beam current.

The beam was passed through a self-supporting gold target approximately 5.3 mg/cm^2 thick, prepared by vacuum evaporation of gold onto a glass slide coated with BaCl, and then floating the gold foil off the slide. The target thickness corresponds to an energy loss of 16 MeV for a 37.5-MeV ^{19}F beam, with a full width at half maximum of about 3 MeV. The ^{19}F nuclei which were Coulomb excited in the gold target were polarized in a direction parallel to the vector $\vec{p}_f \times \vec{p}_i$, where $\vec{p}_f$ and $\vec{p}_i$ are the final and initial momentum vectors of the scattered and excited ^{19}F nuclei. Appendix 1 describes the magnitude of the polarization expected from Coulomb excitation theory, and briefly explains the process. If no nuclear interactions contribute to the population of the 110-keV level, Coulomb excitation theory predicts an average polarization, P_C, of 0.89 in a direction perpendicular to the reaction plane, for the recoils from $\theta_F = 12.5^\circ$ to 50°.

For particles scattered at all φ_F angles (using now a polar coordinate system in which the z axis is parallel to the beam and the x axis is up as shown in Figure 2) there is no net polarization in any direction. In this experiment the ^{19}F nuclei were scattered into a magnetized iron host lattice which precessed the polarization at the

FIGURE 2

Coordinate system used in this thesis.

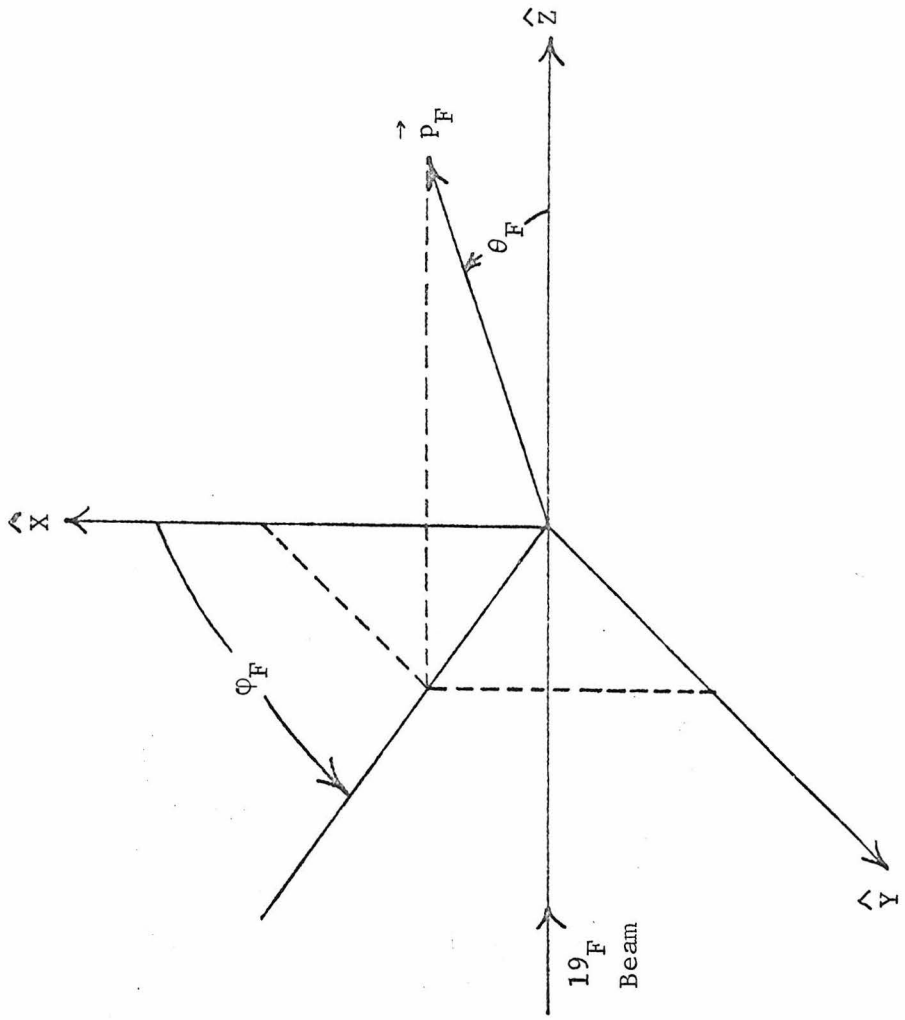

FIGURE 2

Larmor frequency, ω_L, in a plane perpendicular to the beam axis. The Larmor frequency is defined by

$$\hbar\vec{\omega}_L = -g\mu_N \vec{H},$$

where $\vec{H}$ is the magnetic field at the ^{19}F nucleus, g is the so-called g-factor ($=\vec{\mu}\hbar/\vec{I}\mu_N$), $\vec{I}$ is the nuclear angular momentum, $\vec{\mu}$ is the magnetic moment of the state, and μ_N is the nuclear magneton. Those ^{19}F nuclei scattered with φ_F angles between 18° and 162° were stopped in iron with a magnetic field parallel (or anti-parallel) to the beam axis while those recoiled in φ_F angles from 198° to 342° were stopped in iron with a magnetic field in the opposite direction. Those scattered between 342° and 18° and between 162° and 198° were stopped in a non-magnetic material. The two γ-ray detectors described below were mounted at $\theta_F = 90^\circ$, $\varphi_F = \pm 90^\circ$. The magnetic field rotated the oriented $^{19}F^*$ nuclei in such a way that there was a net positive polarization facing one detector and a net negative polarization facing the other detector. Reversing the magnetic field reversed this polarization component.

The component of the polarization directed toward one detector is given by;

$$P = \bar{P}_C \sin(\omega_L t),$$

where t is the time elapsed since the excited ^{19}F entered the iron lattice, and $\bar{P}_C$ is the net polarization for all $^{19}F^*$ nuclei stopping in the iron from $\varphi_F = 18^\circ$ to $\varphi_F = 162^\circ$, reduced by the fraction of

$^{19}F^*$ nuclei which stopped in non-magnetic regions.

$$\bar{P}_C = \left[\frac{P_C}{180^\circ} \int_{18^\circ}^{162^\circ} \sin(\varphi_F)\, d\varphi_F \right] = 0.605\ P_C = 0.54 \ .$$

With a mean lifetime for the excited state of τ, the average polarization for all decays inside the iron is,

$$P = \bar{P}_C \frac{\omega_L \tau}{1 + \omega_L^2 \tau^2} \ .$$

An excitation function for the 110-keV γ radiation was taken, using the same experimental setup as used in the parity experiment, to make sure that the excitation process does not show resonances signifying nuclear interactions. A target 320 $\mu g/cm^2$ thick (approximately 1 MeV) was used and Figure 3 shows the yield of 110-keV γ radiation as a function of the lab energy of the ^{19}F projectile. The energy range studied was from 19.5 to 38.5 MeV. No resonances are seen and the yield varies with energy approximately as expected from Coulomb excitation theory. This is not unexpected since the laboratory Coulomb energy barriers of ^{19}F as a projectile and ^{197}Au and ^{56}Fe as targets are 92 and 48 MeV, respectively. The incident ^{19}F beam energy was 37.5 MeV in the parity experiment, well below half the Coulomb barrier for fluorine on gold, and the scattered ^{19}F nuclei entered the iron with an energy of about 21 MeV, which is also well below half the Coulomb barrier.

The ^{19}F particles with multiple scattering angles in the

FIGURE 3

Excitation function for Coulomb excitation of ^{19}F projectiles on a gold target. The projectile energy is in units of MeV (lab).

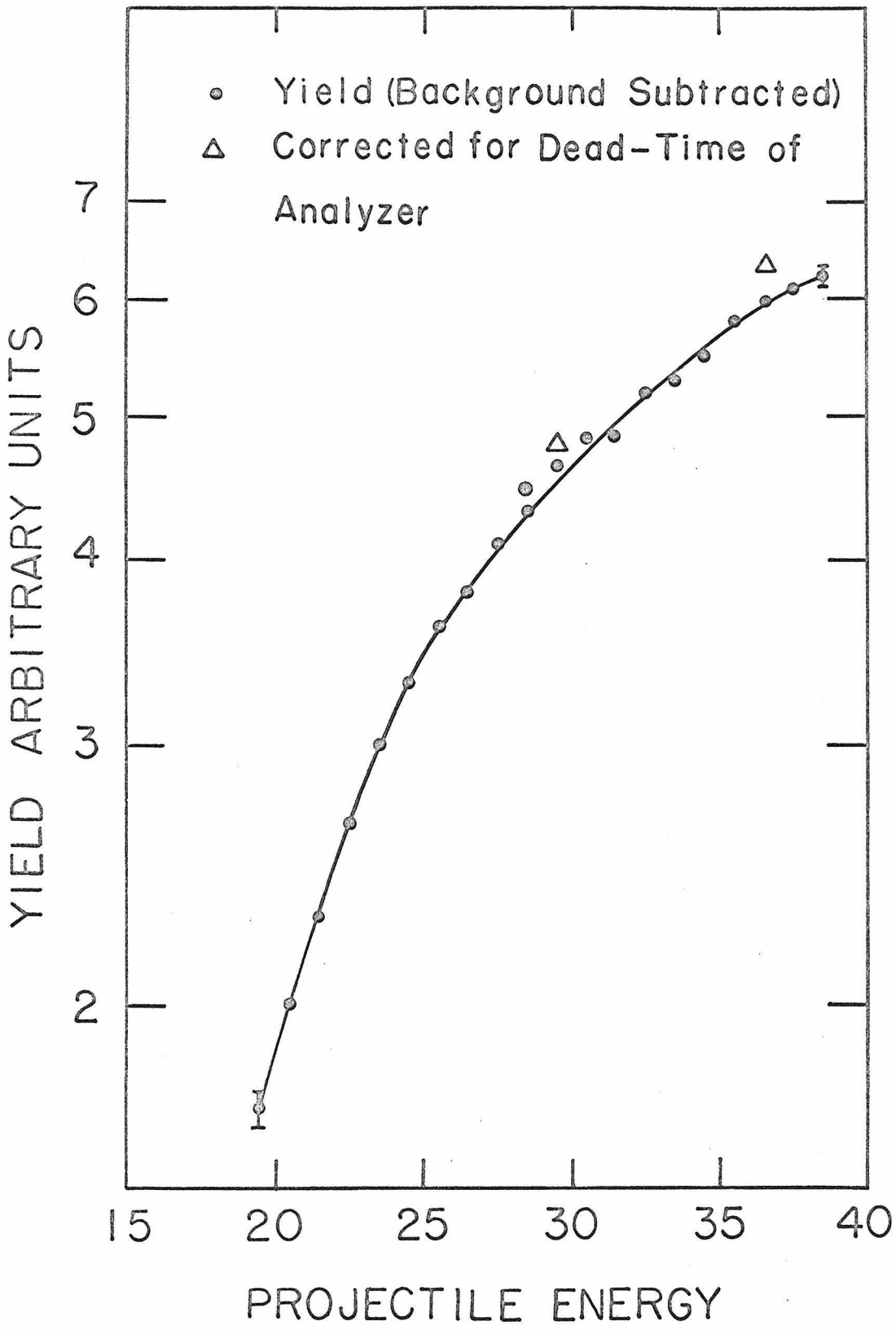
Yield (Background Subtracted)
Corrected for Dead-Time of Analyzer
YIELD ARBITRARY UNITS
2
3
4
5
6
7
15
20
25
30
35
40
PROJECTILE ENERGY

FIGURE 3

target of less than 6^{o} were collected in a gold-plated cup, 7.6 cm in diameter and 6.4 cm deep. The cup was placed 40 cm downstream from the target and the detectors were shielded by lead from γ radiation originating in the cup. No suppression voltage was placed on the cup, but the cup was, instead, connected directly to the beam current integrator which has a very low input impedance. The cup gave grossly incorrect readings if biased with plus or minus 300 volts. Without suppression, the current read by the cup agreed within 20 percent with the current read by a cup, 5 cm in diameter and 46 cm deep, with the direct unscattered ^{19}F beam entering it.

B. Target and Support

Due to the critical importance of maximum possible yield, a rather thick target was used for the parity experiment. Gold was selected because of its high thermal conductivity, high Z, and absence of low-lying states which might be Coulomb-excited and thus create additional background. For 1 μampere of charge-5 beam, more than 3 watts are dissipated in the target in an area of 0.45 square mm. This area establishes an upper limit of 1.2 μampere of $^{19}F(5^{+})$ beam current to prevent melting of the gold target. Platinum was seriously considered as a target material since it has a much higher melting point, but ^{195}Pt has excited states at 99 and 129 keV which would have prevented the extraction of the 110-keV γ-yield with sufficient precision.

It was necessary to bond the gold target to a support having a low thermal impedance to the outside of the scattering chamber.

If the gold targets were floated onto a clean support, using distilled water and conventional techniques, the targets melted at a current of one-fourth to one-tenth of the calculated value.

A channel of copper, having twenty 0.070-inch holes exactly 1/8" apart machined in it, was attached to a 1/2" diameter brass rod which passed through an O-ring seal in lucite, to the outside of the chamber. This allowed many targets to be made from a 1" by 1/8" strip of gold foil, and it also allowed the target to be changed easily from outside of the vacuum system. The beam spot could be viewed on a thin, small piece of quartz mounted on the holder, and by positioning a blank hole in place of the target, the beam current hitting the target holder could be measured to check for incorrect alignment. A silver-base printed circuit repair paint was painted around the edge of the foil after floating it onto the target holder. Some targets were floated directly onto a surface having wet silver paint on it. This procedure also gave good results, with no visible residue on the surface of the foil, but the former method of applying the paint after positioning the foil allowed the foil to be positioned properly after floating it onto the support.

Both methods worked very well and the targets were able to withstand the calculated limit of a uniform 2-MeV, ^{4}He test beam (about 2 μampere). There was still some accidental loss of targets caused by the ^{19}F beam being unintentionally focused to a very small diameter spot.

Target destruction from excessive beam-current was largely

eliminated by the construction of a beam-current discriminator which magnetically interrupted the incoming beam if the beam current on the target exceeded a preset value. The discriminator triggers a silicon-controlled rectifier which in turn energizes a magnet located just after the tandem regulating slits. The system was then manually reset after the beam was reduced to a safe level at the ion source. If the beam-current was still excessive the circuit would interrupt the beam again immediately. The discriminator proved to be very valuable in saving targets since the ^{19}F beam current tended to fluctuate in magnitude during the necessarily long experimental runs.

C. Magnetic Stopper and Support

The Coulomb-excited $^{19}F^*$ nuclei which were scattered between $\theta_F = 12^\circ$ and 50° were stopped in an iron "host" in which the hyperfine field at the $^{19}F^*$ nucleus was used to precess the spin vector of the $^{19}F^*$, and the angular distribution of the decay γ radiation which is, of course, related to the spin direction. Those scattered between $\theta_F = 50^\circ$ and 90° were stopped in a region of uncertain magnetic alignment.

The stopper magnet is shown in detail in Figure 4 and its position with respect to the collimators is shown in Figure 5. To obtain opposite directions for the magnetic fields seen by two ^{19}F recoils with a φ_F difference of 180°, the iron stopper was fabricated in the shape of a cylinder with slits along the length, forming two thin-walled half-cylinders connected at each end with a region of larger cross section. By winding two sets of two turns at each end,

FIGURE 4

Top view of the stopper magnet and support structure.

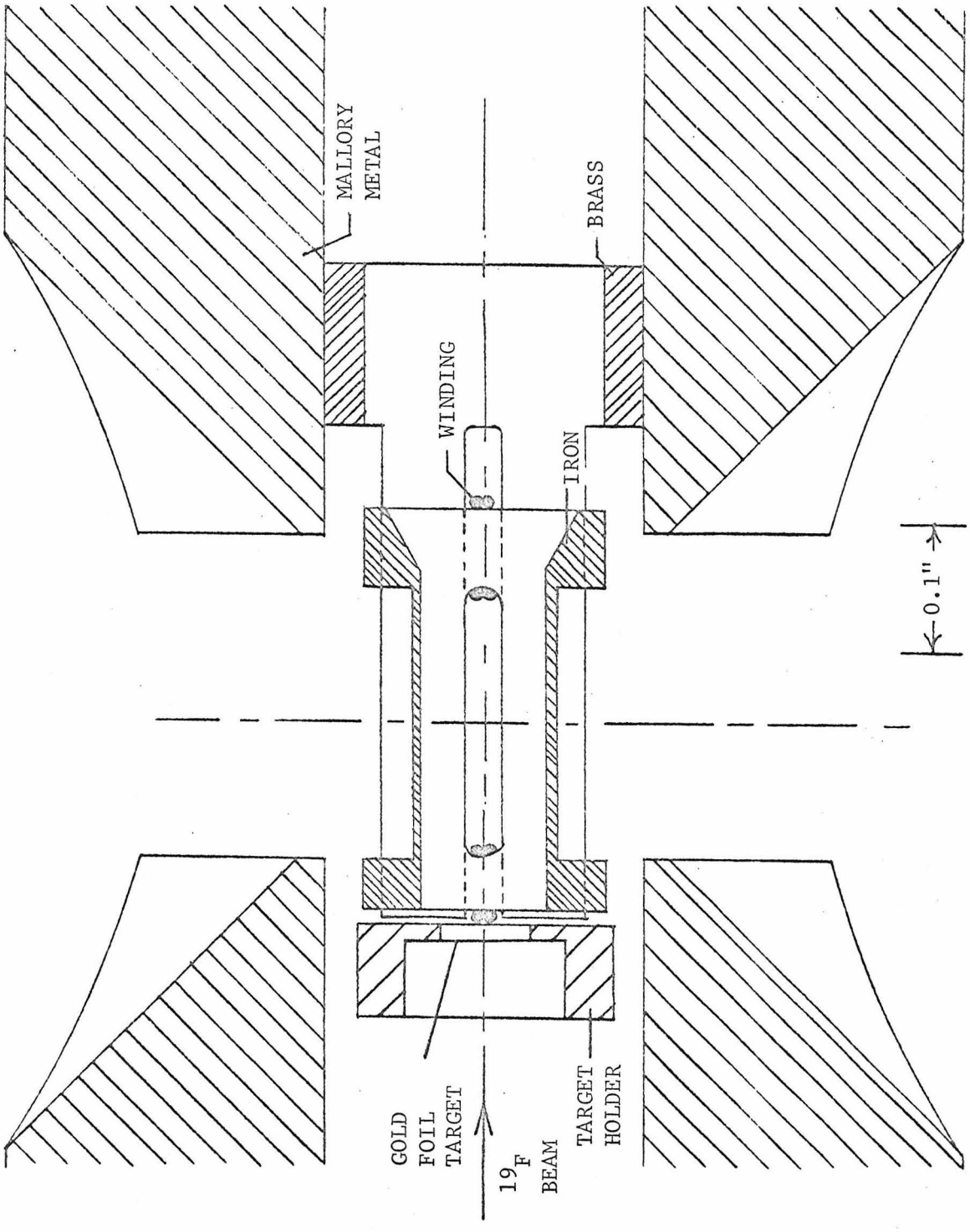
MALLORY METAL
BRASS
WINDING
IRON
0.1"
GOLD FOIL TARGET
19_F BEAM
TARGET HOLDER

FIGURE 4

FIGURE 5

Top view of the beam collimators and other equipment.

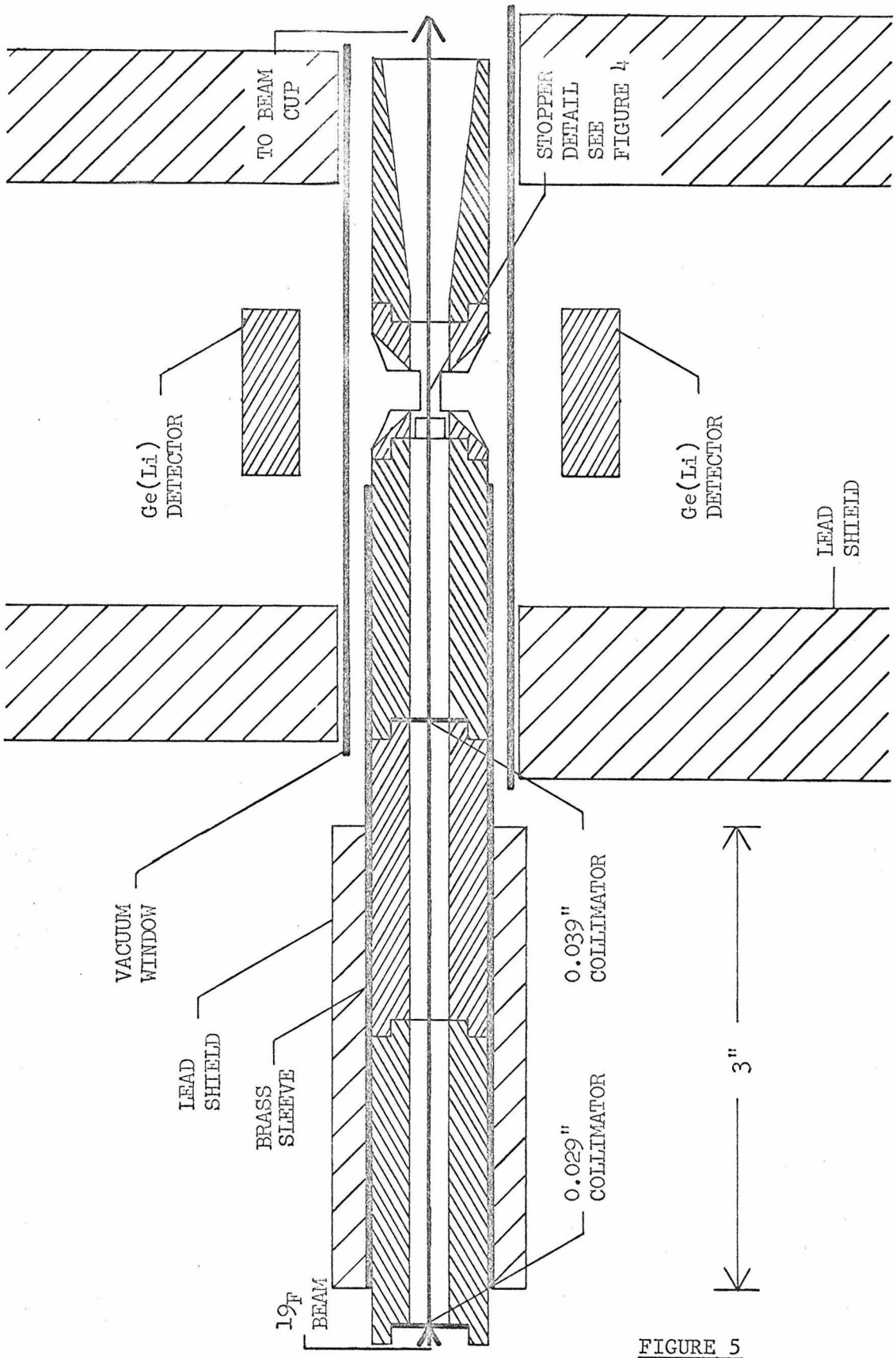
TO BEAM CUP
STOPPER DETAIL SEE FIGURE 4
Ge(Li) DETECTOR
Ge(Li) DETECTOR
LEAD SHIELD
VACUUM WINDOW
LEAD SHIELD
BRASS SLEEVE
0.039" COLLIMATOR
0.029" COLLIMATOR
3"
19F BEAM

FIGURE 5

as shown in Figure 6, the half-cylinders were magnetized in opposite directions. This gave a total of four turns to excite the magnetic field in the stopper. The inner radius of the cylinder was $1\frac{1}{4}$ mm and the wall thickness was about 0.1 mm. The length of the magnetized iron was 5 mm.

For a null experiment, the iron stopper was plated on the inside with more than 15 mg/cm^2 of copper. (The maximum range of ^{19}F nuclei of the appropriate energy in copper was 3 mg/cm^2.) Thus the ^{19}F* nuclei were stopped in the copper, and by making the same measurements with the copper-plated stopper as with the unplated stopper, a check of the basic symmetry of the system was obtained. The results are given in Part IV.

The iron stopper-cylinder was held in a brass holder which was, in turn, placed in a tungsten support as shown in Figure 5. This support was machined from Mallory Metal No. 1000 (Mallory Metal Co.) to absorb 197-keV photons from the decay of the second excited state of ^{19}F. The Coulomb excitation of the 197-keV level is an electric quadrupole (E2) excitation and is therefore not strongly forward-peaked. Most of these ^{19}F* (197 keV) nuclei stop inside the tungsten support. Absorption of the 197-keV γ radiation was especially important for the circular polarization measurements described in Part V.

The design of the iron stopper was chosen to meet several requirements. First, the asymmetry to be measured was expected to be very small. Thus, magnetic fields external to the iron must be as small as possible to avoid deflecting the beam or scattered ^{19}F* nuclei.

FIGURE 6

Stopper magnet with heavy lines indicating the excitation coil.

The iron was annealed in a hydrogen atmosphere as follows. (A standard Commercial process)

Held for four hours at 1175^{o}C

Cooled at 83^{o}C/hr to 590^{o}C

Cooled between 83^{o}C/hr and 122^{o}C/hr to 315^{o}C

Air cooled retort to room temperature.

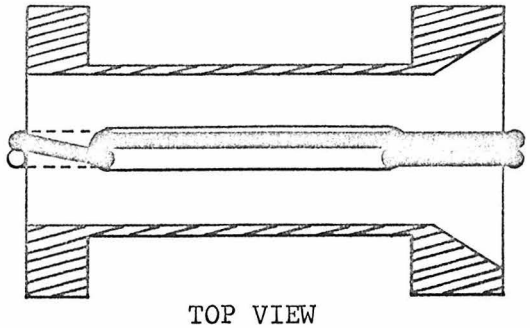

TOP VIEW

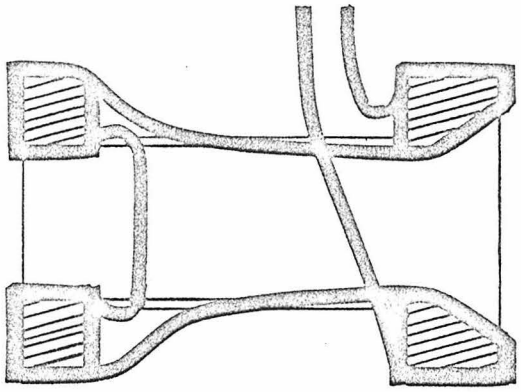

SIDE VIEW

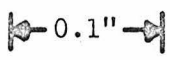

FIGURE 6

This was achieved by fabricating the unit out of a single piece of very pure iron. The unit was then hydrogen-annealed following the procedure indicated in the caption of Figure 6, by a commercial firm. This cleaned the surface and minimized the number of ampere-turns necessary to saturate the iron. The parity runs were made with either 0.25 or 0.5 amperes in the windings, although 0.2 amperes were sufficient to saturate the iron. This produced horizontal fields at the ends of the assembly of about one gauss, but the average field seen by the ^{19}F beam which passed through the length of the cylinder was very small due to the fact that the field direction was in opposite directions at opposite ends of the assembly. The excited ^{19}F nuclei saw a magnetic field of the order of one gauss in a horizontal direction, but this field bends them in a vertical plane, which should not create any asymmetry. Even with an average vertical component of the stray field of one gauss over a one centimeter path (which is a gross overstatement) the maximum asymmetry which would be created by the magnetic field altering the effective source position would be $< 10^{-6}$. This is to be compared with our achieved statistical precision of $\approx 3 \times 10^{-5}$.

Second, the flight path for the scattered $^{19}F^*$ nuclei should be as short as possible to minimize the fraction which decay in flight. With a mean life of 0.88 ns, an average of the values, 0.92 (0.04)* ns (Gale and Calvert, 1963) and 0.84 (0.04) ns (Bougnot et al., 1965), the 21-MeV $^{19}F^*$ recoils have a mean flight path of 1.3 cm before

*Standard errors are given in parenthesis here, and in the rest of the thesis.

decaying.

Third, the fraction of the excited $^{19}F^*$ nuclei collected in the aligned iron lattice should be as high as possible. As shown in Figure 7, the Coulomb excitation cross section ($d\sigma/d\theta_F$) is strongly peaked near 20°. In the geometry used in this experiment, more than 50 percent of the $^{19}F^*$ (110 keV) produced are directed toward the aligned iron lattice; 80 percent of these enter the iron before decaying.

D. γ-Detection and Electronic Circuitry

The γ rays were detected using two nearly identical 6-cc Ge(Li) Ortec planar detectors having FET (Field-Effect Transistor) preamps mounted directly on the cryostat to minimize input capacitance and leakage. The electronic circuits associated with the storage of the spectra and the switching of the magnetic field are shown in Figure 8 and a typical spectrum is shown in Figure 9. Since there was background radiation present, strong efforts were made to achieve the best possible resolution, consistent with the goal of obtaining the most rapid data collection possible.

Ge(Li) detectors were used to eliminate the gain shifts usually produced in the photomultiplier tubes of scintillation counters by varying magnetic fields, such as the magnetic field exciting the stopper magnet. In fact, the background was flat enough in the pulse-height spectra that this would probably not have been a serious problem. Also, the stray magnetic fields were so low that it would have been easy to shield against them.

FIGURE 7

Computed Coulomb excitation differential cross section for 30-MeV ^{19}F on a gold target. The upper curve shows $d\sigma/d\theta$ which is of interest for a cylindrical stopper.

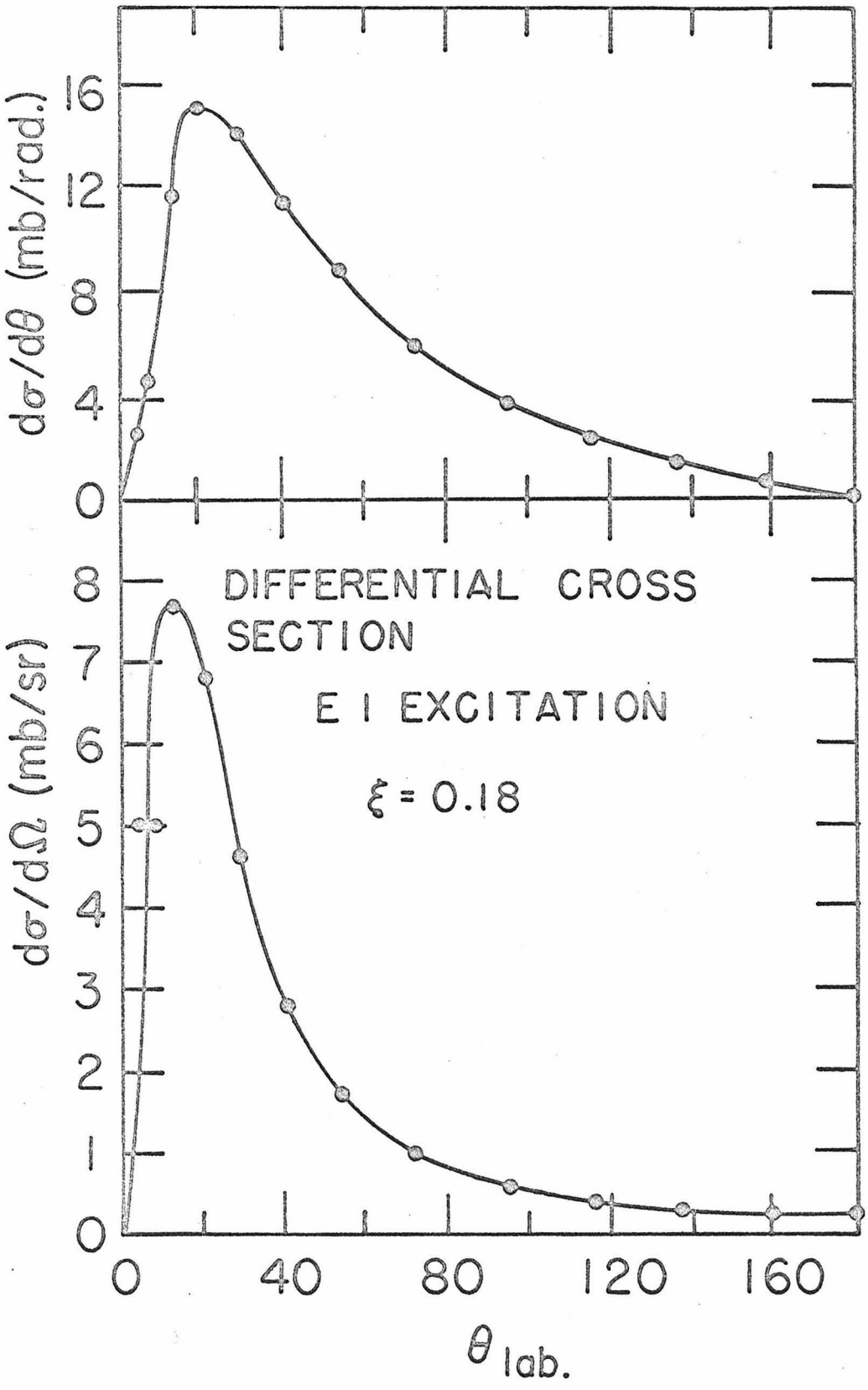
dσ/dθ (mb/rad.)
16
12
8
4
0
DIFFERENTIAL CROSS SECTION
E 1 EXCITATION
ξ = 0.18
dσ/dΩ (mb/sr)
8
7
6
5
4
3
2
1
0
0
40
80
120
160
θ lab.

FIGURE 7

FIGURE 8

Block diagram of the electronic circuits used for the parity search.

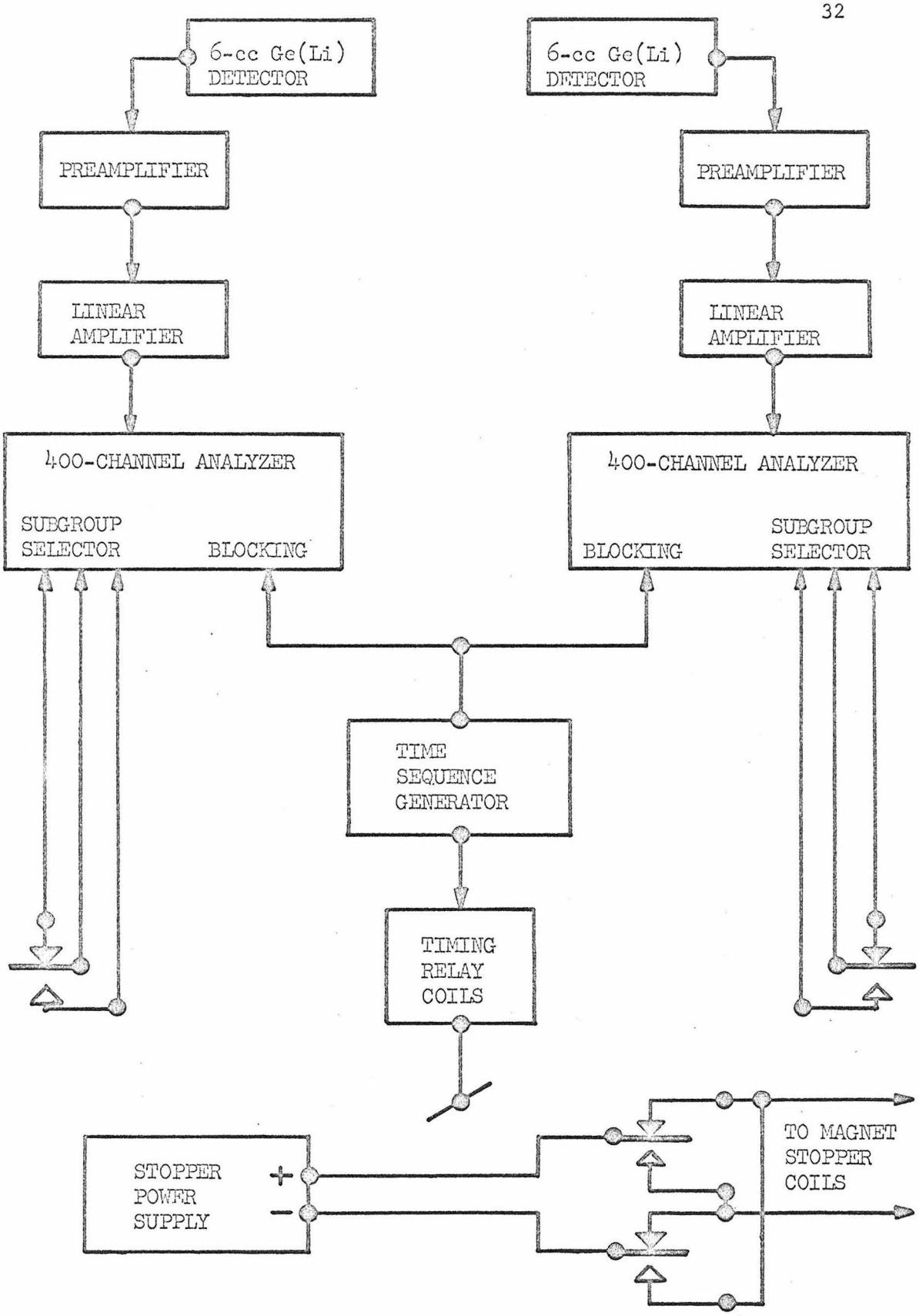
6-cc Ge(Li)
DETECTOR
6-cc Ge(Li)
DETECTOR
PREAMPLIFIER
PREAMPLIFIER
LINEAR
AMPLIFIER
LINEAR
AMPLIFIER
400-CHANNEL ANALYZER
SUBGROUP
SELECTOR
BLOCKING
400-CHANNEL ANALYZER
BLOCKING
SUBGROUP
SELECTOR
TIME
SEQUENCE
GENERATOR
TIMING
RELAY
COILS
STOPPER
POWER
SUPPLY
+
−
TO MAGNET
STOPPER
COILS

FIGURE 8

FIGURE 9

Gamma-ray energy spectra recorded for run No. 388.

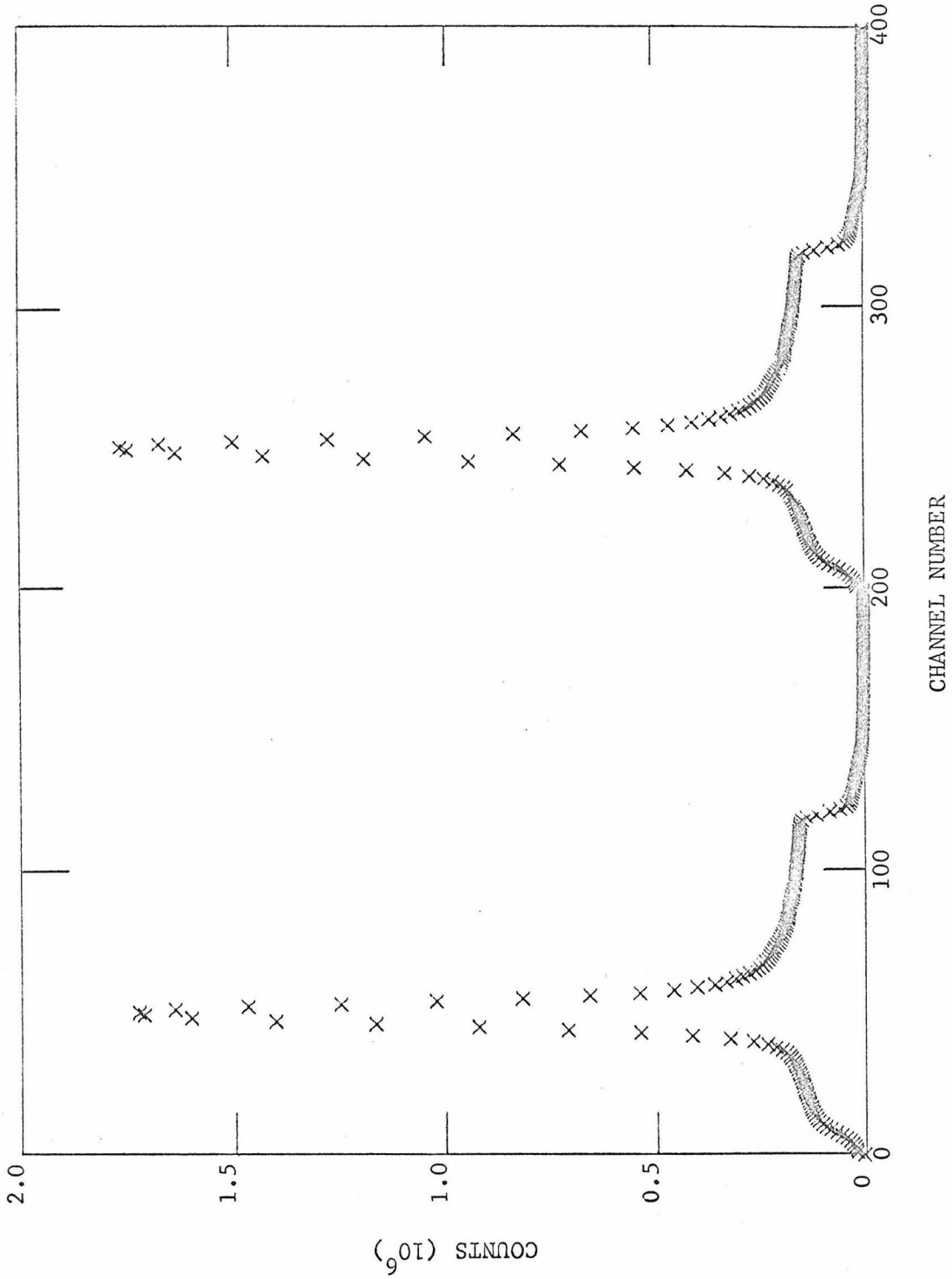

FIGURE 9

The energy region of interest of the γ-spectrum was spread over 200 channels of a 400-channel analyzer to eliminate the analyzer storage time for events of no interest, and to increase the total number of counts in the 110-keV peak which the analyzer could store. The analyzer memory was allowed to overflow on the 10^6 digit to increase the run times to eight hours. The runs were then stored on paper tape and the computer later restored the millions-digit for the channels which overflowed.

Two detectors were placed at symmetrical locations with respect to the asymmetry to be measured so that the detectors could be used to normalize each other as described in Appendix 2. The spectrum from one detector was stored in half of one 400-channel analyzer, and the spectrum from the other detector was similarly stored in half of a second 400-channel analyzer. The selected 200-channel subgroups of both analyzers were externally switched between the two halves of the analyzer memories simultaneously, by the reversing relay driving the magnetic field. A blocking pulse was generated by a time-sequence-generator and applied to the analyzers for 50 ms to block storage of data while the magnet current was being switched. The field direction was changed at a rate of 76 times a minute throughout each eight-hour run. On alternate eight-hour runs the polarity of the voltage on the reversing relay driving the stopper coil was reversed. This entire procedure eliminated possible systematic effects arising from asymmetries in the system, such as slightly different efficiencies in the two 200-channel subgroups of a single analyzer.

The two detectors viewed the magnet stopper through 1-mm thick aluminum vacuum windows as shown in Figure 5. Lead surrounded the detectors to attenuate γ radiation from the room background, the beam cup, and the beam collimators.

E. Scattering Chamber

The above tungsten assembly had two beam collimators mounted in it as shown in Figure 5. The first collimator was 0.029-inches in diameter and a second "anti-scatter" collimator with a 0.039-inch diameter hole in it was mounted about 3" after the first. The assembly, which was made in interlocking pieces, fitted into a brass sleeve which ensured correct axial alignment. Lead was then placed around this to further attenuate γ radiation from the collimators. In spite of the shielding, it was found necessary to clean carbon deposits off of the collimators periodically, to avoid background radiation in the γ-ray circular polarization experiment described in Part V.

The assembly was mounted in a 6x6x12" rectangular scattering chamber with provisions for holding the detectors. A liquid nitrogen trap was mounted just below the tungsten support to minimize carbon deposition on the gold target or the $^{19}F^{*}$ stopper magnet.

With the system completely assembled a telescope was used to double-check the axial alignment and adjust the vertical position of the target holder.

IV. EXPERIMENTAL RESULTS

Table 1 lists the ratio $Q = (N_1^+/N_1^-)/(N_2^+/N_2^-)$, as defined in both Part III and Appendix 2, for all runs taken during the parity experiment for both positive and negative currents. The run numbers are in chronological order. The host was iron (Parity Stopper No. 9) for the data taken for the parity experiment, and copper (plated on an iron stopper) for the null experiment. The current given is that in the four-turn coil on the stopper magnet. For a negative g-factor for the $^{19}F^*$ (110 keV) level, the polarization is positive for detector No. 1 when the current is positive and the field reversing relay is in the "+" position.

The experimental ratios are given for three regions of the γ-ray energy spectrum. Q(Low) was computed for the energy region just below the 110-keV region, Q(110 keV) was computed for the energy region of interest, and Q(High) was computed for the energy region just above the 110-keV region.

The Q's were averaged, grouping similar runs together and the results of the averaging are shown in Table 2. If $Q_A(Q_B)$ is the computed Q for a current greater (less) than zero, then $\delta = (Q_A/Q_B - 1)/8$. The statistical uncertainty in δ is $\sigma(\delta) = (\Sigma\, 1/N)^{\frac{1}{2}}/8$, where the sum extends over the eight numbers entering into the ratio Q_A/Q_B. The δ's for each set are shown in Table 2 along with the average for similar sets, yielding the "final averages." In all cases the statistical uncertainty is included in parenthesis.

TABLE 1

Summary of parity experiment runs where Q is defined in the text.

RUN	HOST	CURRENT	Q(Low)	Q(110 keV)	Q(High)
383	IRON	.25	1.00154 (.00118)	1.00095 (.00050)	1.00209 (.00113)
384	IRON	-.25	1.00301 (.00116)	1.00075 (.00049)	1.00103 (.00112)
385	IRON	.25	.99987 (.00116)	1.00088 (.00051)	1.00171 (.00111)
386	IRON	-.25	1.00530 (.00113)	1.00085 (.00046)	1.00278 (.00109)
387	IRON	.25	1.00145 (.00113)	.99991 (.00046)	1.00139 (.00110)
388	IRON	-.25	1.00291 (.00112)	1.00026 (.00047)	1.00092 (.00110)
389	IRON	.25	1.00183 (.00111)	1.00144 (.00046)	1.00000 (.00106)
390	IRON	-.25	1.00171 (.00110)	1.00069 (.00047)	1.00151 (.00105)
391	IRON	.25	1.00216 (.00110)	1.00081 (.00046)	1.00007 (.00105)
392	IRON	-.25	.99997 (.00107)	1.00011 (.00045)	1.00121 (.00102)
393	IRON	.25	1.00199 (.00105)	1.00114 (.00046)	1.00117 (.00100)
394	IRON	-.25	1.00147 (.00215)	1.00046 (.00095)	1.00033 (.00206)
413	IRON	.50	1.00001 (.00112)	.99998 (.00048)	1.00390 (.00110)
414	IRON	-.50	1.00137 (.00097)	1.00113 (.00040)	1.00470 (.00096)
415	IRON	.50	1.00086 (.00138)	1.00145 (.00056)	1.00262 (.00136)
424	COPPER	.50	1.00140 (.00112)	1.00100 (.00044)	1.00534 (.00110)
425	COPPER	-.50	1.00085 (.00124)	1.00077 (.00049)	1.00211 (.00121)
426	COPPER	.50	1.00044 (.00114)	1.00123 (.00045)	1.00543 (.00112)
427	COPPER	-.50	1.00080 (.00122)	1.00101 (.00049)	1.00282 (.00119)
428	COPPER	.50	1.00058 (.00135)	1.00094 (.00055)	1.00509 (.00132)
429	COPPER	-.50	.99759 (.00144)	1.00062 (.00057)	1.00545 (.00143)

TABLE 2

Average of Data in Table 1

Set	Runs
1	383, 385, 387, 389, 391, 393
2	384, 386, 388, 390, 392, 394
3	413, 415
4	414
5	424, 426, 428
6	425, 427, 429

Set	Host	i	Q(Low)	Q(110 keV)	Q(High)
1	Iron	+.25	1.00151 (0.00046)	1.000852 (0.000193)	1.00104 (0.00044)
2	Iron	-.25	1.00246 (0.00049)	1.000521 (0.000204)	1.00143 (0.00047)
3	Iron	+.5	1.00035 (0.00087)	1.000603 (0.000364)	1.00339 (0.00086)
4	Iron	-.5	1.00138 (0.00097)	1.001130 (0.000400)	1.00470 (0.00096)
5	Copper	+.5	1.00084 (0.00069)	1.001070 (0.000273)	1.00531 (0.00067)
6	Copper	-.5	0.99996 (0.00074)	1.000817 (0.000296)	1.00324 (0.00073)

Set	Host	|i|	δ(Low) $\times 10^{-5}$	δ(110 keV) $\times 10^{-5}$	δ(High) $\times 10^{-5}$
1&2	Iron	.25	-11.8 (8.3)	4.13 (3.51)	-4.9 (8.0)
3&4	Iron	.5	-12.8 (16.3)	-6.59 (6.76)	-16.2 (16.1)

Final Average		δ(Low) $\times 10^{-5}$	δ(110 keV) $\times 10^{-5}$	δ(High) $\times 10^{-5}$
5&6	Copper	11.0 (12.7)	3.16 (5.03)	25.7 (12.4)
1-4	Iron	-12.0 (7.4)	1.9 (3.1)	-7.2 (7.2)

The χ^2 for the six final averages shown in Table 2 is 9.4 if it is assumed that each δ should really be zero. The probability of a $\chi^2 \geqslant 9.4$ is 0.15, for this assumption.

The background in the γ-ray energy spectrum (Figure 9) originates from many sources. Some of the γ-radiation background sources are; a) the collimators, b) scattered ^{19}F beam hitting the beam tube, c) Coulomb-excited ^{19}F(197 keV), etc. Since the source of the radiation is not known in detail, there is no compelling reason to expect these background sources to be self-normalizing, as the 110-keV radiation is. For example, the yield from background which is created by long lived radioactive substances being produced by the beam on the collimators will be proportional to the time the analyzer is in one 200-channel subgroup and not necessarily proportional to the beam charge as the 110-keV radiation is.

In the experiment using the copper stopper, the background amounted to 1/6.25 of the counts in the integrated 110-keV peak, and this ratio was 1/5.55 for the iron stopper data. The data from the runs on the copper stopper indicate that the asymmetry of the background cannot be interpreted as a mechanical or electronic asymmetry of our counting system since the average asymmetry of the background is $18.5(8.9) \times 10^{-5}$ while the asymmetry of the 110-keV radiation is only $3.2(5.0) \times 10^{-5}$. The background therefore has a "real" asymmetry which reverses with the magnetic field, etc. For this reason, the fraction of the background asymmetry which would lie in the region of the 110-keV peak was subtracted from the 110-keV data. This yields

a value for the quantity δ(Adjusted) of $3.6(3.2) \times 10^{-5}$ for iron as a host lattice and $0.2(5.2) \times 10^{-5}$ for copper as a host.

As stated in Part III, the theoretical asymmetry is related to δ. With a measured angular distribution of $1 + \delta \cos(\theta_\gamma)$, $P\eta = \delta'$ where δ' is the asymmetry of the 110-keV γ radiation with experimental factors unfolded. The following list indicates the corrections which relate the corrected asymmetry to the asymmetry measured in this experiment. (These factors could be considered as reductions in the polarization, P.)

1) The 110-keV γ radiation accounts for 84 percent of the radiation in the integrated region. $\delta \rightarrow \delta/0.84$
2) 68(5) percent of the detected 110-keV γ radiation originates from $^{19}F^*$ scattered between θ_F angles of 12° and 50° which enter the host before decaying. The remainder either decay in flight, or stop in other unmagnetized regions where the detector can see the γ-decay radiation. $\delta \rightarrow \delta/0.68$
3) The γ-ray detectors subtend a cone angle of 27°. $\delta \rightarrow \delta/0.95$

The result of the above corrections is that $\delta' = \delta/0.54$. Thus, $\eta = (\delta/0.54)/P$.

From Part III, $P = 0.54 \dfrac{\omega_L \tau}{1+(\omega_L \tau)^2}$. If the magnetic field seen at the nuclei of the implanted $^{19}F^*$ ions is H_5 (measured in units of 100 kgauss; hence, the term H_5), the expected value of P is $0.54 \times 0.239 \dfrac{H_5}{1+0.06\ H_5^2} = 0.129 \dfrac{H_5}{1+0.06\ H_5^2}$. This assumes a mean life

for the 110-keV level of 0.88 ns. It also assumes that the g-factor of the 110-keV state is g = - 0.566 (Maqueda, 1966).

If a distribution of fields exists, with a fraction f(H) of the $^{19}F^{*}$ nuclei in each field, then

$$P = 0.129 \sum \frac{H_5 \, f(H_5)}{1 + 0.06 \, H_5^2} \ ,$$

where the sum extends over all hyperfine fields. It should be noted that $\Sigma \, f(H) = 1$.

Using the values for δ(Adjusted) and P given above, the resultant η values are:

$$\eta = 5.2 \ (4.6) \times 10^{-4} \sum \frac{1 + 0.06 \, H_5^2}{H_5 \, f(H_5)} \quad \text{for iron, and}$$

$$\eta = 0.3 \ (7.5) \times 10^{-4} \sum \frac{1 + 0.06 \, H_5^2}{H_5 \, f(H_5)} \quad \text{for copper.}$$

V. HYPERFINE MAGNETIC FIELD MEASUREMENTS

From Part IV, it is clear that the average value of the hyperfine field at the $^{19}F^{*}$ nuclei implanted in an iron lattice is needed to compute a physically meaningful result for the parity admixture.

There are several general methods for measuring nuclear hyperfine fields, of which the most important methods are listed below.

1) The Mössbauer effect is utilized to observe the hyperfine energy splitting of nuclear levels.
2) A level is produced with a non-isotropic angular distribution and fast-timing techniques are used to observe a time-differential rotation of the angular distribution at the Larmor frequency of the implanted excited nucleus.
3) A level is produced with an angular distribution and the integral rotation of the angular distribution (integrated over the lifetime of the level) is observed.
4) NMR techniques are used to destroy a nuclear alignment and thus an angular distribution.

Methods 1, 2, and 4 yield information about unique values of hyperfine fields found at the nuclei of an impurity atom in a host lattice but it is difficult to extrapolate to an average field since many different hyperfine fields may be present. This thesis includes a paper by the author and collaborators, as Appendix 3, which shows

that there are at least two hyperfine fields seen by fluorine in nickel, but only about one-half of the total asymmetry is precessed by these two fields. The remainder of the asymmetry may be in higher field components, in no field, or in a distribution of fields so that no single component contains an amplitude large enough to be detected. Although the unique fields are of interest from a solid-state physical standpoint, the value of the average hyperfine field is needed for experiments similar to the parity experiment described here.

The results for the hyperfine fields in nickel are also of interest here since they may indicate what to expect for hyperfine fields of fluorine in iron. The two hyperfine fields in nickel were observed at 17.8 kG and 90.2 kG. Since the crystal structure of iron and nickel are body-centered cubic and face-centered cubic, respectively, it is not unreasonable to assume that iron behaves similarly to nickel with hyperfine fields scaled up by the ratio of the average magnetic moment per electron outside of the filled "3p" sub-shell.* This would imply fields in iron at 82 kG and 420 kG. We have observed a hyperfine field in iron, using the technique described in Appendix 3, of about 92 kG with between 1/4 and 1/10 of the total

---

*At present the mechanism which produces hyperfine fields is not understood sufficiently well to predict the exact ratio between hyperfine fields in nickel and iron. The average magnetic moment per atom could be used to scale the fields but this would predict fields in iron of 0.8 times the fields quoted here. On the other hand, the actual observed field in iron is 1.1 times the scaled field given here.

asymmetry precessed by it. The time resolution was not sufficiently short to observe fields above approximately 150 kG, but no hyperfine fields of less than 92 kG were found.

Method 3 above would give exactly the information needed for the parity experiment if the product of the lifetime and g-factor of the state used was the same as the product for the 110-keV level of ^{19}F. This method was therefore utilized to obtain information about the average hyperfine field for fluorine in an iron host, but the distribution of fields was not obtainable using it.

As mentioned in Appendix 3, if a magnetic field is perpendicular to the plane defined by the axis of nuclear alignment (the beam axis for these measurements) and the direction of the decay photon, the time-dependent angular distribution of the γ radiation is given by

$$W(\theta,t) = 1 + B_2 \cos(2\theta + 2\omega_L t) + B_4 \cos(4\theta + 4\omega_L t),$$

where $\hbar\omega_L = -g\mu_N H$, and B_2, B_4 are the coefficients of the unperturbed angular distribution.

Integrating $W(\theta,t)$ over the lifetime of the nuclear level gives

$$\begin{aligned} W(\theta,H) &= 1/\tau \int e^{-t/\tau} W(\theta,t)\, dt \\ &= 1 + B_2 \frac{(\cos(2\theta) - 2\omega_L\tau\sin(2\theta))}{1 + (2\omega_L\tau)^2} \\ &\quad + B_4 \frac{(\cos(4\theta) - 4\omega_L\tau\sin(4\theta))}{1 + (4\omega_L\tau)^2} \quad . \end{aligned}$$

If the magnetic field direction is periodically switched, as in the parity experiment, then the ratio

$$2\,\frac{W(\theta,+H)\ -W(\theta,-H)}{W(\theta,+H)\ +W(\theta,-H)} = \frac{2\omega_L\tau}{1+(2\omega_L\tau)^2}\,\frac{dW(\theta,0)}{d\theta}\,\frac{1}{W(\theta,0)}\,[1 + 0\ ((\omega_L\tau)^2)]$$

$$\approx \frac{2\omega_L\tau}{W(\theta,0)}\,\frac{dW(\theta,0)}{d\theta} \equiv 2\omega_L\tau\ S\ ,$$

where S is the fractional slope at the angle θ. Since $(\omega_L\tau)^2 \ll 1$ as shown below, the higher order term was neglected.

If a distribution of hyperfine fields exists, then $2\omega_L\tau$ must be replaced by

$$\frac{\sum \frac{2\omega_L\tau\ f(H)}{1+(2\omega_L\tau)^2}}{\sum \frac{f(H)}{1+(2\omega_L\tau)^2}}$$

where f(H) was defined in Part IV as the fraction of fluorine nuclei in each field, H. This correction was also neglected but ω_L must be replaced by its average,

$$\overline{\omega_L} = \sum f(H)\omega_L\ .$$

A. Experimental Method

The ONR-CIT tandem accelerator was used to produce a $^3He^+$ beam with an average current of 0.7 μA, on a 100 μg/cm^2 thick, SiO target, evaporated <u>in vacuo</u> on an iron or copper backing. The

reaction $^{16}O(^{3}He,p)^{18}F^{*}$ was utilized to populate the 937-keV, $J^{\pi} = 3^{+}$, state of ^{18}F. The level diagram for ^{18}F is shown in Figure 1. The experimental mean life of this state is 68(7) ps (Alexander et al., 1966) and its g-factor has been calculated by A. P. Shukla (1968) using a wave function consisting of two particles in the s-d shell. He obtained the value, $g = +0.61$, which he found was quite insensitive to the details of the wave function.

The p-γ coincidence technique was used, with protons back-scattered between 163° and 173°, to obtain a strong angular distribution in the γ-decay, and to reduce background in the γ-spectra. The protons were detected in an annular surface-barrier Si detector with an active area of 50 mm^2 and a depleted depth of 300 μm, using a single-channel analyzer to select the proton group of interest. An aluminum foil 0.001-inch thick was placed in front of the particle detector to absorb the elastically-scattered ^{3}He. The γ rays were detected in two Ge(Li) detectors (having 20-cc and 5-cc active volume, respectively) and the signals were fed through two linear gates before being stored in two 400-channel analyzers. A diagram of the electronics for the magnetic field measurements is shown in Figure 10.

An excitation function was taken for the above conditions, counting for two intervals, one with the detector placed at 0° and the other with the detector placed at 45°. The ratio of the counts at the two angles gives a measure of the asymmetry. A beam energy of 3.78 MeV was selected because there appeared to be a maximum in the asymmetry at that energy, and the yield was also near a maximum at

FIGURE 10

Block diagram of the electronic circuits used for the magnetic field measurements. Note that linear gates external to the 400-channel analyzer were used. This eliminated any difference in the linear gate internal to the analyzer which might be a function of the subgroup used. Small gain shifts were noticed (a minute fraction of a channel) when the internal gate was used.

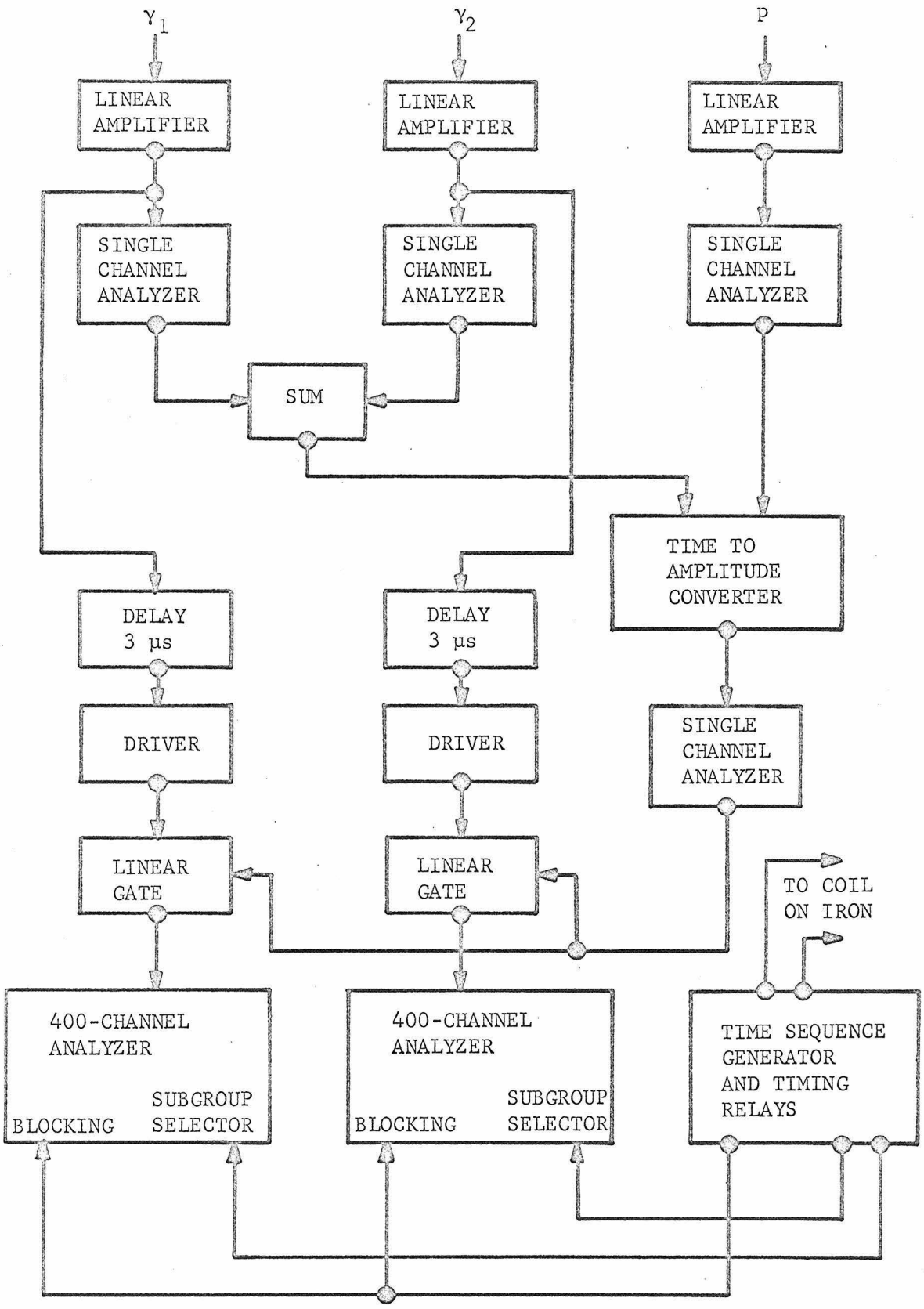
γ_1
γ_2
P
LINEAR AMPLIFIER
LINEAR AMPLIFIER
LINEAR AMPLIFIER
SINGLE CHANNEL ANALYZER
SINGLE CHANNEL ANALYZER
SINGLE CHANNEL ANALYZER
SUM
TIME TO AMPLITUDE CONVERTER
DELAY 3 μs
DELAY 3 μs
DRIVER
DRIVER
SINGLE CHANNEL ANALYZER
LINEAR GATE
LINEAR GATE
TO COIL ON IRON
400-CHANNEL ANALYZER
BLOCKING
SUBGROUP SELECTOR
400-CHANNEL ANALYZER
BLOCKING
SUBGROUP SELECTOR
TIME SEQUENCE GENERATOR AND TIMING RELAYS

FIGURE 10

3.78 MeV.

Before measuring the unperturbed angular correlation of the 937-keV γ radiation, the angular symmetry of the experimental setup was checked by measuring the angular distribution of the delayed annihilation γ radiation from the β^+-decay of the ^{18}F produced by the ^3He beam. ($\tau(^{18}F) \approx 159$ minutes) A brass plug was inserted behind the radioactive region of the target and the copper target support was covered with 0.01 inch of copper to ensure that all β^+ were stopped near their point of origin. The 511-keV γ radiation had to pass through a 0.02-inch thick sheet of copper perpendicular to the beam axis. The yield of 511-keV radiation was normalized to a fixed NaI(Tl) crystal at 80^o, to correct for radioactive decay. The apparent angular distribution of the 511-keV radiation in the Ge(Li) detector compared very well with that expected due to the γ-ray attenuation as a function of angle in the copper. One useful feature of this method of checking the angular symmetry is that the annihilation radiation is formed essentially at the exact spot where the ^3He beam bombards the target.

The unperturbed angular distribution of the 937-keV γ radiation was measured with the 20-cc Ge(Li) detector at 11 cm from the target, in coincidence with the back-scattered-proton detector. For this measurement the 100 $\mu g/cm^2$ SiO target was evaporated on a 0.01-inch thick copper strip. The angular distribution is, after a small correction for the γ-ray attenuation in the 0.01-inch thick copper target backing,

$$W(\theta) = 1 + A_2 P_2(\cos\theta) + A_4 P_4(\cos\theta),$$

where $A_2 = 0.23(0.02)$ and $A_4 = -0.08(0.02)$, which yields a fractional slope at 45^o of

$$S = 0.27(0.02)/\text{radian}.$$

Pure, annealed iron was then used as a target backing to observe a rotation of the angular distribution. The two detectors were placed at θ angles of plus and minus 45^o, and the field alternately reversed in a direction perpendicular to the plane defined by the two γ-detectors and the target. The quantity

$$\delta = [(N_1^+/N_1^-)/(N_2^+/N_2^-) - 1]/4$$

was computed, where $N_{1,2}^{+,-}$ is the yield for detector 1,2 while the external field is up (+) or down (-). As can be easily seen from the algebra presented earlier,

$$\delta = \bar{\omega}_L \tau S = \bar{\omega}_L \tau 0.27(0.02)/\text{radian}.$$

For g = 0.61 and a mean life of 68(7) ps,

$$\bar{\omega}_L \tau = 1.99(0.20) \times 10^{-2} H_5$$

where H_5 is the average hyperfine field measured in units of 10^5 gauss. Thus,

$$\delta = 5.4(0.7) \times 10^{-3} H_5 .$$

B. Experimental Results

The following pieces of iron were run with various excitation currents. The results are tabulated in Table 3.

Sample 1 was a 0.01-inch thick, one-inch long, iron foil clamped in a magnetic yoke having a 1000 turn winding on it.

Sample 2 was identical to Sample 1.

Sample 3 was the magnetic stopper used in the parity experiment (Stopper No. 9). The target was evaporated on the outside of its cylindrical surface and the stopper was excited by the same four-turn coil as used in the parity experiment.

Sample 4 was a 0.01-inch thick, 0.25-inch wide, 1-inch long iron strip excited with current flowing directly through the strip, along the long direction of the strip.

The following should be noted from the data presented in Table 3. The average of Sample 1 and 2, with at least 0.05 A in the coil, is $\delta = 4.7(0.8) \times 10^{-3}$. The average of Sample 3 with excitation currents between 0.25 A and 0.5 A is $\delta = 2.3(0.8) \times 10^{-3}$. There is no indication that the effect increases as the current in the coil of Sample 3 is increased above 0.2 A. There is also no indication that the asymmetry decreased as the amount of ^{3}He entering the foil increased; these results are, however, not sensitive to possible changes in the iron which occurred during the first few hours of bombardment. The effect in Sample 4 for a current of about 4 A is

TABLE 3

SUMMARY OF DATA FROM THE MAGNETIC FIELD MEASUREMENTS

Sample	Current A	$\delta(10^{-3})$
1	0.025	0.7(1.8)
	0.037	2.9(1.8)
	0.05	5.9(1.8)
	0.1	5.2(1.7)
	0.2	4.8(1.9)
	0.3	3.0(1.9)
2	0.5	4.8(1.6)
	0.5	4.5(2.5)
3	0.03	1.3(1.7)
	0.1	-1.5(1.6)
	0.2	2.2(2.2)
	0.25	4.8(1.5)
	0.33	0.6(1.4)
	0.5	1.9(1.3)
	0.7	-0.8(2.6)
	1.0	1.7(2.7)
	1.8	1.7(2.7)
4	2.0	-0.4(3.9)
	4.0	1.5(1.3)
	6.5	-0.3(1.7)
	17.6	2.6(1.0)
	20.0	1.0(1.4)

$\delta = 0.7(1.0) \times 10^{-3}$ and it increases to $2.1(0.8) \times 10^{-3}$ for a current of approximately 17 A. Using the formula in Section A of this part of the thesis the following magnetic fields are obtained.

For Sample 1 and 2 $H = 0.88(0.19) \times 10^5$ gauss, and

for Sample 3 $H = 0.43(0.16) \times 10^5$ gauss.

It was assumed that $(\omega_L \tau)^2$ was small in the above calculations. In fact, $\bar{\omega}_L \tau \sim 2 \times 10^{-2}$. For an extreme magnetic field distribution, the average field being produced by 1/10 of the fluorine nuclei seeing $10H_5$, $\omega_L \tau$ would be approximately 0.2 and including the higher order terms would increase the average field by $\approx$ 1 percent for this experiment.

The above data can be understood if the assumption is made that the "annealing" of the iron is partially or totally destroyed by radiation damage from the ^3He beam which passes through the region of the iron where the recoil $^{18}F^*$ nuclei stop. The coincidence-selected ^{18}F nuclei recoil into a forward cone with a half-angle less than 10^o. This hypothesis was checked by the following experiment.

1500 Å of pure iron was evaporated onto a glass slide which was in an external magnetic field and held at 400^o C during the evaporation. The iron covered a 1-cm diameter round spot on the glass slide. The glass slide and the iron were coated with 5 $\mu g/cm^2$ of gold to form a conducting layer from the iron to a brass support for the glass slide. The support for the slide acted as a beam cup.

A beam of 100-keV $^{19}F^-$ ions from the tandem-accelerator

negative-ion source was collimated using a $\frac{1}{2}$-inch diameter hole and a movable wire probe checked the uniformity of the beam. The iron film, with no applied magnetic field on it, was bombarded with the ^{19}F beam which has a calculated projected range of about 1200 Å in the iron with a straggle of about 600 Å (Schiott, 1967). After bombardment, the magnetization, M, was measured as a function of applied field, H, for various quantities of integrated beam charge hitting the iron spot.

The results of these M vs. H measurements are shown in Figure 11. It is of interest to note that, although the shape of the M-H curve changed as the dosage increased, the magnetic excitation needed to saturate the iron did not change appreciably until between 2×10^{16} and 7×10^{16} $^{19}F/cm^2$ penetrated the iron. Then a drastic change occurred, the iron requiring a much higher excitation to obtain saturation. The actual bombardment doses were probably somewhat higher than the quoted doses, since some of the $^{19}F^-$ beam ions were neutralized by the residual gas in the beam tube. The pressure at the start of a bombardment was less than 2×10^{-5} torr, decreasing to about 10^{-6} torr during the run.

If the cross section for the displacement of iron atoms from the lattice is assumed to be limited by the Thomas-Fermi screening radius,* and if it is further assumed that two lattice sites are ruined by one iron atom being displaced, the bombardment for which

---

*For a cut-off of 60-eV energy transfer to the iron atom, the Rutherford cross section for 100-keV ^{19}F on iron is much larger than this limit.

FIGURE 11

Magnetization curves for a 1500Å thick iron film as a function of 100-keV, ^{19}F beam damage. The vertical axis is the bulk magnetization of the sample and the horizontal axis is the applied magnetic field. The horizontal scale is 2.5 Oe/large division. The radiation dose increases for the lower inserts. Note that two orientations of the sample developed. Insert D and E are for the same radiation dose but the sample was rotated in the curve tracer to obtain the largest slope (D) and smallest slope (E) for the knee.

Insert	Approximate dose $^{19}F/cm^2$	
A	0	
B	4×10^{12}	
C	2×10^{13}	
D,E	6×10^{13}	
F,G	3×10^{14}	
H,I	1×10^{15}	
J,K	4×10^{15}	
L,M	2×10^{16}	
N,O	7×10^{16}	
P	7×10^{16}	as N but with the applied magnet field increased by a factor of 3.

FIGURE 11

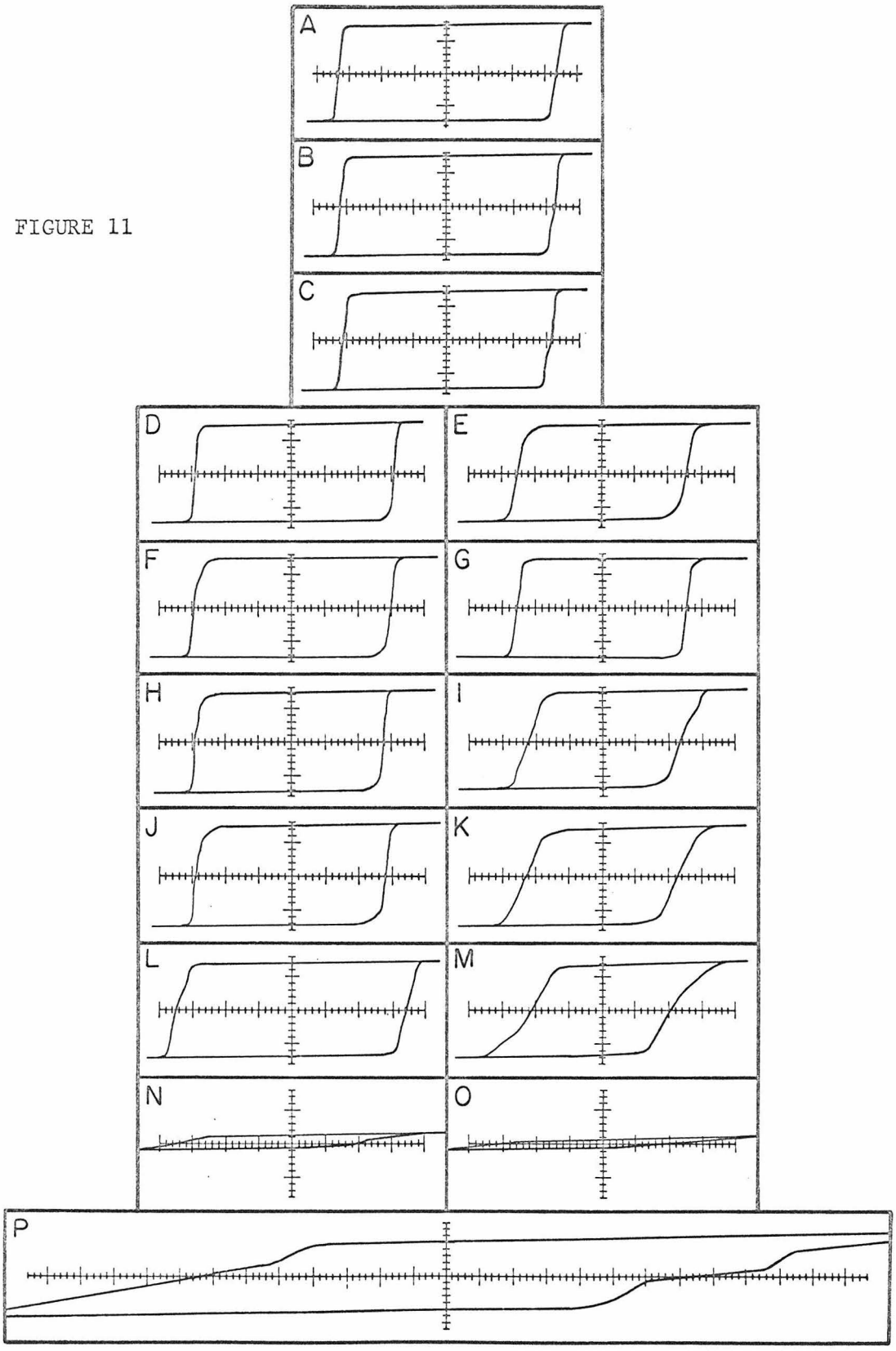

there is a pronounced change in the M-H curve corresponds to approximately 20 percent to 60 percent of the iron sample being disordered. Extrapolating to what one could expect from a 3.78-MeV ^{3}He beam, by using the Rutherford cross section and an energy cutoff of 60-eV transfer to the iron atom to displace it, the effective permeability of the iron should be altered to a similar extent after 1 to 3 hours of bombardment by a 1 μA ^{3}He beam, on a 1-mm^2 spot.

It is therefore concluded that the reduced asymmetry for Sample 3 above, and probably also for Sample 4, is due to a reduction in the effective permeability caused by radiation damage, and an insufficient magnetic excitation field to saturate the disordered iron.

C. Circular-Polarization Experiment

The parity-violation effect is proportional to the net polarization of the $^{19}F^{*}$ (110 keV) nuclei. The γ rays from a decay between two $J = \frac{1}{2}$ states will have a circular polarization equal to the polarization of the initial state along the photon momentum axis. Thus, if the circular polarization of the 110-keV decay γ rays is measured, it is unnecessary to know the g-factor of the excited state or the average hyperfine field in iron separately. An attempt was made to measure this and although it suffered from a large statistical uncertainty, it confirmed the above results.

Two transmission-type γ-ray polarimeters were used to measure the circular polarization of the 110-keV γ radiation from the parity stopper magnet. The experimental setup was identical to the

parity experiment except a polarimeter was placed in front of each 6-cc Ge(Li) γ-detector.

The polarimeters consisted of a projected length (to the photons) of 0.81 cm of a magnetically saturated iron alloy (2 percent vanadium, 49 percent cobalt, and 49 percent iron). The direction of the magnetization of the polarimeter was switched and the difference in the transmission (due to changes in the Compton scattering of the photons) was measured for both positive and negative currents in the parity stopper. This method has been discussed by many authors; see for example, Steffen and Frauenfelder (1965), Paul et al. (1967), and Chesler (1965). The asymmetry calculated by Paul et al. was used here. The expected asymmetry, A, for 110-keV γ radiation is $-4 \times 10^{-3}P$, where A is defined as $A = (N^{+} - N^{-})/(N^{+} + N^{-})$. $N^{+,-}$ is the yield when the polarimeter magnetization is parallel (+) or anti-parallel (-) to the photon direction. This calculated asymmetry assumes a projected iron thickness of 0.82 cm and a circular polarization of the γ radiation of P.

In this measurement, the plane of the magnetized iron polarimeter was at 45^{o} to the direction of the photons. Corrected for this, and for the fact that the projected thickness of the iron was 0.81 cm, the asymmetry to be expected is $-2.8 \times 10^{-3}P$. The observed asymmetry for 9 days of running was $-1.4(1.0) \times 10^{-4}$ before correcting for the dilution of the asymmetry arising from background. Correcting for the background dilution, the asymmetry equals $-3.3(2.3) \times 10^{-4}$ which implies a polarization, P, of 0.12(0.08).

From Part IV,

$$P = 0.129 \sum \frac{f(H)\ H_5}{1 + 0.06\ H_5^2} \quad .$$

Thus, without knowing what the distribution of fields might be, $H_5 \geqslant 0.99(0.66)$ since any distribution of fields will reduce P below what it would be for a unique field with a value equal to the average of the distribution.

D. Conclusion

The average hyperfine field from the ^{18}F data, is

$$\bar{H} = 0.88(0.19) \times 10^5 \text{ gauss},$$

for fluorine implanted in an iron host, in the absence of radiation damage.

If the reduced average field in the parity stopper (Sample 3, above) is assumed to be associated with some unknown effect other than the radiation damage discussed above, the average field becomes, instead,

$$\bar{H} = 0.43(0.16) \times 10^5 \text{ gauss},$$

since it would then have to be concluded that the reduced field is a property of the material or geometry of the parity stopper.

VI. CONCLUSION

A. Discussion of the Results

The polarization of the $^{19}F^{*}$, measured directly in Part V, is P = 0.12(0.08) (see Page 59). The polarization calculated from the measured hyperfine field of Part V cannot be obtained without making an assumption regarding the distribution, f(H), of the hyperfine fields.

As mentioned in Part V, we have observed a unique hyperfine field of about 92 kG with between 1/4 and 1/10 of the total asymmetry precessed by it. Thus, it cannot be assumed that the average field of 88 kG, observed in the iron foil, is the result of one unique field. The assumption could be made that a distribution of hyperfine field exists around 100 kG with an average of 88 kG.

Another possible assumption is that iron behaves similarly to nickel, and exhibits two hyperfine fields with a ratio of 5 in their strengths (the same ratio as between the two nickel fields). If it is assumed that 25 percent of the fluorine nuclei see a 92 kG field, then 14 percent of the fluorine could be in a 460 kG field, creating an average field of 88 kG. It is of interest to note that this fraction of fluorine in the higher field (5 × 92 kG) is nearly the same fraction as the fraction of fluorine in the higher field observed in nickel (Appendix 3).

The first assumption above leads to a polarization of the

$^{19}F^*$ of $0.129 \frac{0.88}{1 + 0.04} = 0.109(0.023)$, while the second assumption leads to an average polarization of

$$P = 0.129 \left[\frac{0.25 \times 0.92}{1 + 0.05} + \frac{0.14 \times 4.6}{1 + 1.2} \right] = 0.066(0.014) \ .$$

It seems reasonable to assume that the field distribution lies somewhere between the two discussed above but since there is no compelling reason to choose one distribution over the other, the results below are based on the assumption that the average field is generated by a reasonably narrow distribution of hyperfine fields.

One of two conclusions can be drawn for the parity violation effect measured by this experiment. Either $\eta = 6.1(5.6) \times 10^{-4}$, or $\eta = 12(11) \times 10^{-4}$ depending on which value of the magnetic hyperfine field is assumed to be present in the parity stopper.

If the radiation damage in the parity stopper was negligible during the parity run, as indeed seems to be the case, then the field present was probably the larger of the two hyperfine fields, i.e., that measured for Samples 1 and 2, as described in Part V.

Using the Rutherford cross section for scattering at 15^o in gold, the implantation dosage expected in the parity stopper at 15^o is less than 10^{16} fluorine atoms/cm^2 during the total running time of the parity experiment. This dose rapidly decreases with angle. Also, the implanted ^{19}F ions were spread out in depth in the iron by the range-straggling of the 37.5-MeV ^{19}F ions due to straggle in their energy loss in the gold target and also in the iron. Since

the threshold for significant damage in 1500 Å of iron (approximately 120 $\mu g/cm^2$) is greater than 2×10^{16} fluorine atoms/cm^2, and the energy straggle in the gold target alone is about 3 MeV (about 1 mg/cm^2 of range in iron), it seems safe to assume that the critical dosage was not reached in the parity experiment, even at 15°.

Thus, the measured value for a $1 + P\eta \cos\theta$ angular distribution is most probably $\eta = 6.1(5.6) \times 10^{-4}$.

This result excludes the a priori possibility that the parity impurities of the nuclear levels are much larger than that calculated by Maqueda using the weak-interaction theory (i.e., $|\eta| = 4.3 \times 10^{-4}$). To measure a parity impurity at the level predicted by the weak-interaction theory, a considerable improvement in precision is needed. It appears that the present experiment is capable of the improved precision if the statistical accuracy of the data can be improved by a factor of about four.

B. Suggestions for Improvement

Recent calculations by McKellar (1968) indicate that the theoretical parity-violating effects calculated using Michel's potential should be reduced by a factor between 1/3 and 1/2 due to the hard-core (short-range repulsive force) which is characteristic of recent nucleon-nucleon potentials, at least for the heavy nuclei he considered. This has to be kept in mind when one explores the possibility of reducing the experimental uncertainty to a level where a more stringent test of theory would be possible. There are, however, several direct ways to improve the experiment.

To increase the yield of 110-keV photons, higher energy ^{19}F beams are needed. 37.5 MeV was selected for this experiment since the available beam current dropped rapidly above this energy. Accelerating a charge 5^+ beam, it was necessary to have $6\frac{1}{4}$ MV on the terminal of the tandem accelerator. At times the machine-loading, due to the large input of heavy ions, increased above the capacity of the accelerator charging system, even for a current of only 1 μA on the target.

If a 60-MeV ^{19}F beam could be obtained, the yield could be increased by almost a factor of 4 by using a thicker target. This would also slightly decrease the fraction of the $^{19}F^*$ nuclei which decay in flight, although this was not a serious problem in the present experiment. The polarization of the $^{19}F^*$ would decrease slightly with the increased energy.

The fraction of 2π solid-angle subtended by the γ-detectors was 0.1 for each detector. This fraction could be increased by using larger detectors and including them in the vacuum chamber used to hold the other equipment. A factor of two might be obtainable here.

The dead-time of the 400-channel analyzer was about 50 percent during these runs. Much of the dead-time was produced by pulses outside the energy region of interest. This part of the dead-time could be eliminated by using a biased-amplifier with an upper level discriminator before the analyzer. With an increase of a factor of eight in the count rate, this step might not be sufficient to reduce the dead-time to reasonable limits. Three fast single-channel

analyzers could be used to select the regions of interest, and the counts scaled in a fast scaler.

It is also not unreasonable to consider using NaI(Tl) to detect the γ radiation. If good enough resolution could be obtained to separate the intense, low energy ($\approx$ 84 keV) X rays in the spectra from the 110-keV yield, or shielding used to eliminate them, it would be easy to obtain a larger solid angle for the γ-ray detection.

With these improvements, a value of $\eta < 2 \times 10^{-4}$ could be measured. The g-factor of the 110-keV level could also be measured more accurately using the circular-polarization technique discussed in Part V, if a large enough, accurately-known magnetic field could be produced.

Radiation damage should not increase much if the bombarding energy is increased, to increase the 110-keV γ-ray yield, since the Rutherford cross section decreases with energy, and the spread in depth of the ^{19}F nuclei in the iron is increased for longer ranges by the range straggling.

APPENDIX 1

POLARIZATION FROM COULOMB EXCITATION

For a detailed review of Coulomb excitation theory and experiments, the reader is referred to the literature. (e.g., Alder et al., 1956a.) This appendix will describe briefly the polarization of an excited level by Coulomb excitation as it pertains to the present experiment.

Consider the reaction $i \rightarrow f$, in a coordinate system in which the z axis is perpendicular to the reaction plane (z axis parallel to $\vec{p}_f \times \vec{p}_i$), and the x axis is parallel to the scattered projectile (Figure 12). Let the nuclear charge of the projectile (target) be Z_1 (Z_2), and the atomic numbers A_1 and A_2, respectively.

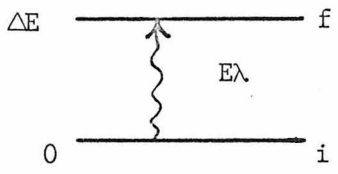

$E\lambda$ is the multipolarity of the excitation and ΔE is the excitation energy of the level. ($\Delta E = E_f - E_i$) Let the change in the z-projection of the nuclear spin be $-\mu$. ($-\mu = M_f - M_i$)

Coulomb excitation theory assumes that the nucleus is excited only by the long-range electromagnetic interaction between the projectile and the target. Thus the two interacting nuclei must remain far enough apart that nuclear forces do not contribute to the interaction. This condition is satisfied if the energy of the incident projectile, E, is considerably below the Coulomb energy barrier, E_C, of the interacting particles. For a nuclear radius of

FIGURE 12

Coordinate system used in Appendix 1.

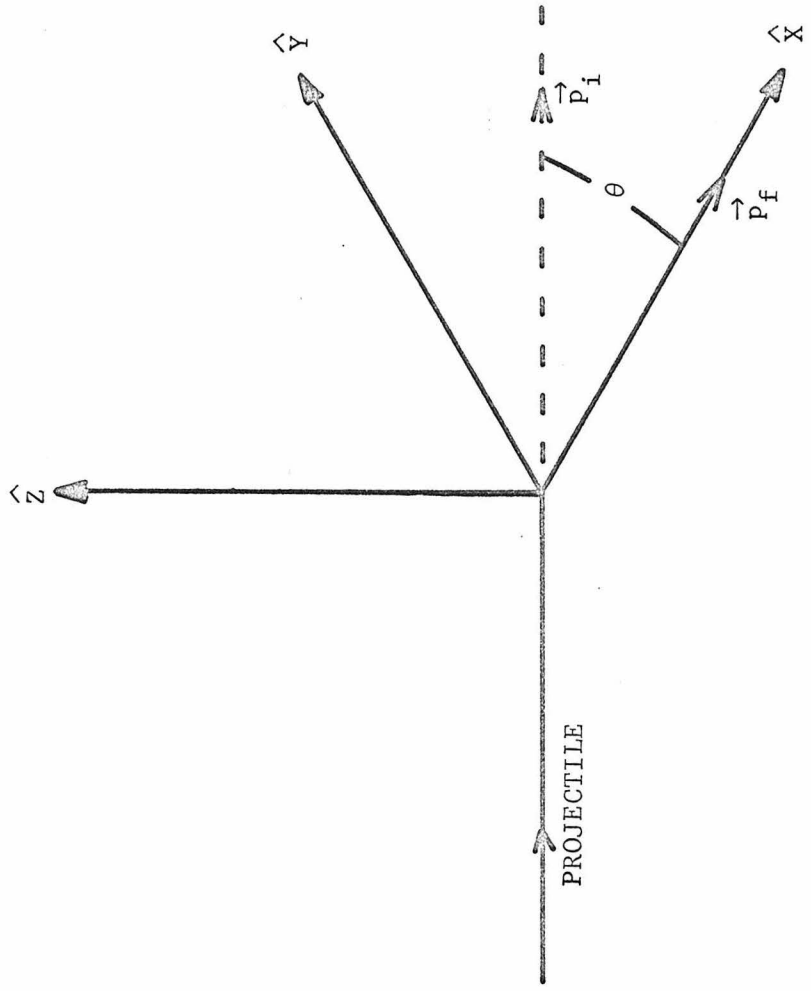

FIGURE 12

$1.44\ A^{1/3} \times 10^{-13}$ cm,

$$E_C = \frac{Z_1 Z_2}{A_1^{1/3} + A_2^{1/3}} \quad \text{(MeV} \tag{1}$$

in the center-of-mass system.

In the limit in which the de Broglie wavelength of the projectile is much less than the distance of closest approach, 2a, and in which the classical orbital angular momentum of the projectile is high, the relationships given below, between excitations which change the projection of the spin of the excited nucleus, can be derived.

The limit on the de Broglie wavelength can be written as (Alder et al., 1956a)

$$\eta = \frac{a}{\lambda\!\!\!^{-}} = \frac{Z_1 Z_2 e^2}{\hbar v} \gg 1, \tag{2}$$

where v is the relative velocity of the two particles. The limit of large classical angular momentum, ℓ, can be expressed as

$$\frac{\ell}{\hbar} = \frac{Z_1 Z_2 e^2}{\hbar v} \cot(\theta/2) \gg 1, \tag{3}$$

where θ is the scattering angle of the projectile. θ should not be confused with the polar angle of the coordinate system used in this appendix.

Using Eq. 2, Eq. 3 can be rewritten as

$$\frac{\ell}{\hbar} = \eta \cot(\theta/2). \tag{4}$$

Using the fine structure constant, α, η can be put into the slightly simpler form,

$$\eta = \frac{Z_1 Z_2}{\beta} \alpha \approx \frac{Z_1 Z_2}{137\beta} , \tag{5}$$

where $\beta = v/c$.

In general, the differential cross section can be written as

$$d\sigma_\mu(\theta) \propto \left| \frac{[(\lambda - \mu)!(\lambda + \mu)!]^{\frac{1}{2}}}{(\lambda - \mu)!!(\lambda + \mu)!!} I_{\lambda\mu}(\theta, \xi) \right|^2 \frac{d\Omega}{\sin^4(\theta/2)} , \tag{6}$$

where

$$\xi = \frac{\alpha Z_1 Z_2 \Delta E'}{\beta\, 2E} \approx \frac{Z_1 Z_2 \Delta E}{137\beta 2E} \quad (1 + \frac{A_1}{A_2}), \quad \text{with } \Delta E' = \Delta E \ (1 + \frac{A_1}{A_2}), \tag{7}$$

and $I_{\lambda\mu}(\theta, \xi)$ is the classical orbital integral for the interaction.

The scattering cross section can be approximated in the limit of large ℓ as

$$d\sigma_\mu(\theta) \propto \left| \frac{[(\lambda - \mu)!(\lambda + \mu)!]^{\frac{1}{2}}}{(\lambda - \mu)!!(\lambda + \mu)!!\epsilon} \Gamma\left(\frac{-\lambda + \mu + 1}{2}\right) W_{-\frac{\mu}{2}, -\frac{\lambda}{2}}(2\xi\epsilon) \right|^2 \frac{d\Omega}{\sin^4(\theta/2)}, \tag{8}$$

for $(\lambda + \mu)$ even, and

$d\sigma_\mu(\theta) = 0$, for $(\lambda + \mu)$ odd,

where $\epsilon = 1/\sin(\theta/2)$, and W is the Whittaker function (Alder et al., 1956a). In the limit, $2\xi\epsilon \gg 1$, the Whittaker function can be expanded to yield (Whittaker and Watson, 1963)

$$d\sigma_\mu(\theta) \propto \left| \frac{[(\lambda - \mu)!(\lambda + \mu)!]^{\frac{1}{2}}}{(\lambda - \mu)!!(\lambda + \mu)!!\epsilon} \Gamma\left(\frac{-\lambda + \mu + 1}{2}\right)(2\xi\epsilon)^{-\mu/2} e^{-\xi\epsilon} \right. \tag{9}$$

$$\left. (1 + 0(\frac{1}{2\xi\epsilon})) \right|^2 \frac{d\Omega}{\sin^4(\theta/2)} ,$$

for $(\lambda + \mu)$ even, and

$d\sigma_{\mu}(\theta) = 0$, for $(\lambda + \mu)$ odd.

From Eq. 9, one can derive the ratio,

$$\frac{d\sigma_{-|\mu|}(\theta)}{d\sigma_{|\mu|}(\theta)} = \left| \frac{\Gamma\left(\frac{-\lambda - |\mu| + 1}{2}\right)}{\Gamma\left(\frac{-\lambda + |\mu| + 1}{2}\right)} \right|^2 (2\xi\epsilon)^{2|\mu|}, \text{ for } (\lambda + \mu) \text{ even.} \tag{10}$$

Thus, when $2\xi\epsilon$ is large, the cross section with the negative μ, and therefore the positive value of $M_F - M_i$, will dominate. Even if the initial state is unpolarized the final state will have a net polarization, for scattering through some angle θ. One can visualize this polarization as being produced by the rotation of the electric field as the two particles pass.

In the table below, the polarization, P, calculated using the above approximations, is compared with that calculated using the classical orbital integrals for $\xi = 0.2$ (Alder and Winther, 1956b). The value of $2\xi\epsilon$ is also given since it is assumed large for the expansion of the Whittaker function.

θ	$2\xi\epsilon$	P(approx)	P(correct)
10°	4.6	0.98	0.98
20°	2.3	0.91	0.95
30°	1.5	0.81	0.90
40°	1.2	0.69	0.85

In the present experiment (37.5-MeV ^{19}F on ^{197}Au), $\eta = 89 \gg 1$.

Figure 13 shows $P(\theta)$ computed from the classical orbital integrals for $0^{\circ} \leq \theta \leq 180^{\circ}$. It must be kept in mind that although $P(\theta) \rightarrow 1$ as $\theta \rightarrow 0$, the differential cross section equals zero at $\theta = 0$, so there is no contradiction with the fact that no scattering plane is defined at $\theta = 0$.

For the experiment at hand, the differential cross section is strongly peaked at 15° (see Figure 7). For the conditions of this experiment, $\xi = 0.18$. The approximation above predicts a polarization of 0.87 for the angle of maximum yield. The average polarization for ^{19}F nuclei scattered from 12.5° to 50°, computed using the Fortran code CL13 (Winther, 1967), is about 0.89.

FIGURE 13

Polarization of the excited projectile after Coulomb excitation. The parameters correspond to approximately 30-MeV ^{19}F projectiles on a gold target, leading to the excitation of a 110-keV level in the projectile by an E1 transition.

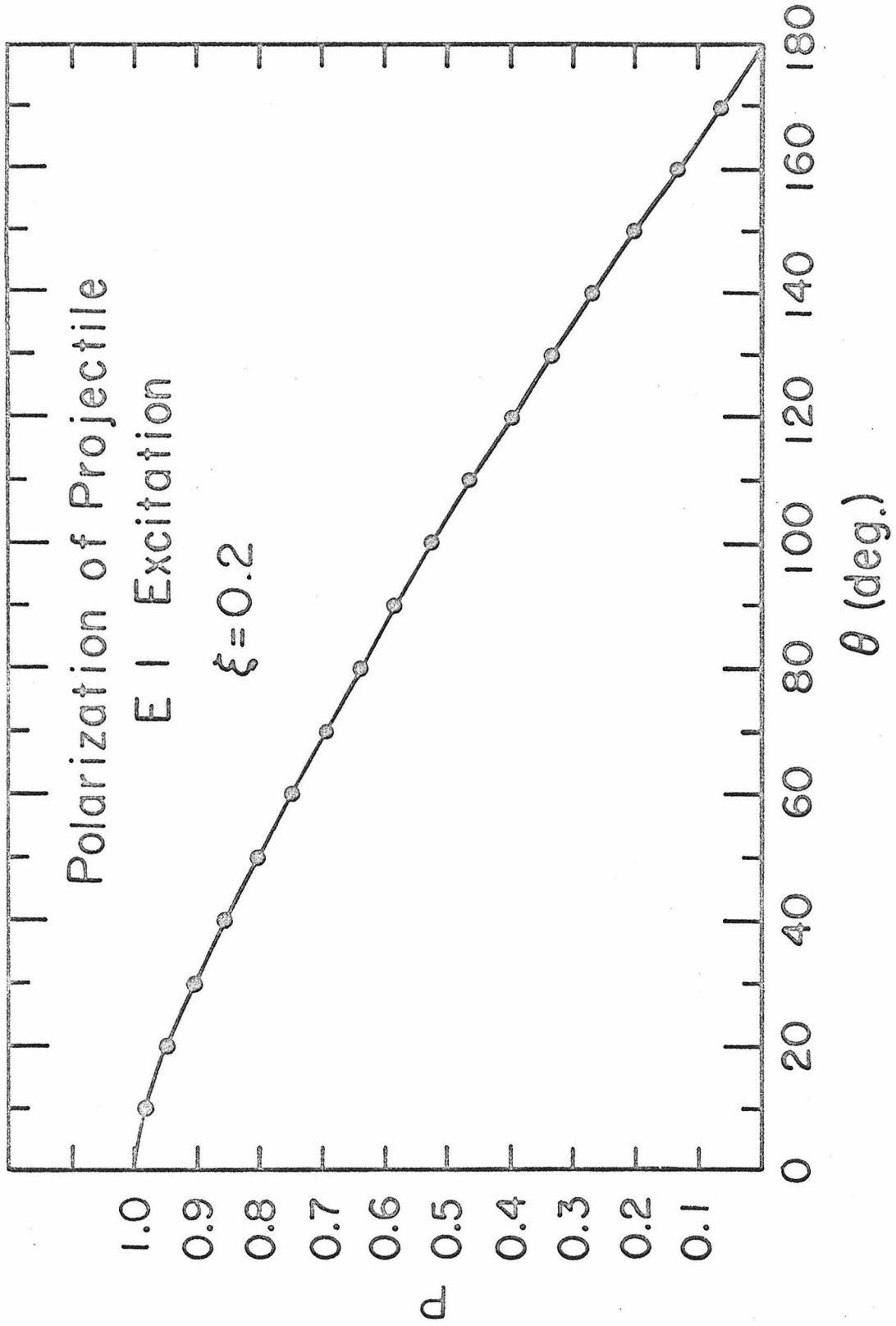
Polarization of Projectile
E I Excitation
ξ=0.2
P
θ (deg.)
1.0
0.9
0.8
0.7
0.6
0.5
0.4
0.3
0.2
0.1
0
20
40
60
80
100
120
140
160
180

FIGURE 13

APPENDIX 2

DEAD-TIME EFFECTS IN ASYMMETRY EXPERIMENTS

Measuring a small asymmetry when an accelerator is the source of the detected radiation introduces a number of problems which do not confront the experimenter using a long-lived radioactive source. The most important of these is the effect of changes in the dead-time of the counting system which can cause false asymmetries.

Consider a general experiment employing an accelerator in which a very small difference in the number of counts is expected when a magnetic field is changed from "up" to "down". With two detectors viewing the same target, at symmetric locations with respect to the effect, the numbers of counts in the two detectors with the field up (+) or down (-) are

$$N_1^{\pm} \propto q_{\pm}\sigma\, T_{\pm}\epsilon_1 R_1^{\pm}\, (1 - D_1^{\pm})(1 \pm \delta_1)$$

and

$$N_2^{\pm} \propto q_{\pm}\sigma\, T_{\pm}\epsilon_2 R_2^{\pm}\, (1 - D_2^{\pm})(1 \pm \delta_2),$$

where

$N_{1,2}^{\pm}$ is the number of events recorded for detector 1,2 during the period ±,

$q_{\pm}$ is the beam charge during the period ±,

σ is the cross section,

$T_{\pm}$ is the target thickness during the period ±,

$\epsilon_{1,2}$ is the product of the solid angle and efficiency of detector 1,2,

$R_{1,2}^{\pm}$ is the intrinsic efficiency of the scaling unit on detector 1,2 for the period ±,

$D^{\pm}_{1,2}$ is the fractional dead-time associated with detector 1,2 during the period ±, and

$\delta_{1,2}$ is the fractional asymmetry in count rate for detector 1,2, which is to be measured.

If the detectors are situated so that $-\delta_2 = +\delta_1 = +\delta$, then

$$Q_A = (N_1^+/N_1^-)/(N_2^+/N_2^-) = \frac{R_1^+R_2^-}{R_1^-R_2^+}\left[\frac{(1 - D_1^+)(1 - D_2^-)}{(1 - D_1^-)(1 - D_2^+)}\right]_A \frac{(1 + \delta)^2}{(1 - \delta)^2} \quad ,$$

where the A denotes experiment "A". If the same experiment is repeated with the phase of the magnetic field reversed with respect to the detectors, then Q_B has the same form as Q_A with $\delta \rightarrow -\delta$ and $A \rightarrow B$. The dead-time factors are, in general, different since they depend on the fluctuations of the beam current. The ratio, Q_A divided by Q_B, reduces to

$$\frac{Q_A}{Q_B} = \frac{\left[\dfrac{(1 - D_1^+)(1 - D_2^-)}{(1 - D_1^-)(1 - D_2^+)}\right]_A}{\left[\dfrac{(1 - D_1^+)(1 - D_2^-)}{(1 - D_1^-)(1 - D_2^+)}\right]_B} \frac{(1 + \delta)^4}{(1 - \delta)^4} \equiv (1 - D)\frac{(1 + \delta)^4}{(1 - \delta)^4} \quad ,$$

where D, substituted for the ratio of the dead-time factors for the two runs, is proportional to the asymmetry caused by the dead-time effects. It should be noted that $\langle D \rangle = 0$. The ratio Q_A/Q_B does not depend on the intrinsic efficiency of the scaling units, but it does assume that the efficiencies do not change between the runs with the field + and -. As mentioned earlier, in this experiment the

field direction was changed 76 times a minute. It was found that $|(R_1^+/R_1^-) - 1|$ was sometimes as large as 10^{-4}, where R_1^+ (R_1^-) was the intrinsic efficiency of channels 0-199 (200-399) of one 400-channel analyzer using a single analogue to digital converter.

For δ and $D \ll 1$,

$$\delta = (Q_A/Q_B)/8 + D/8 \pm \sigma(\delta) ,$$

where $\sigma(\delta)$, the statistical uncertainty in δ, equals $(\Sigma 1/N)^{\frac{1}{2}}/8$, and the sum extends over the eight numbers entering into the ratio.

The probability that a count is lost is proportional to the square of the instantaneous beam current. If the processing (dead) time of an event is τ, then

$$1 - D_1^+ = 1 - \frac{\int \frac{dN_1^+}{dt} \tau_1 \, dq_+}{\int dq_+} ,$$

where the integral is taken over the period during which the field is "+". Since $\frac{dN_1^+}{dt} \propto \frac{i^+ N_1^+}{q^+}$ and $dq^+ = i^+ dt$, we have

$$\frac{1 - D_1^+}{1 - D_1^-} = \frac{1 - \frac{N_1^+ \int i_+^2 dt \, \tau_1}{q^+ \int i_+ dt}}{1 - \frac{N_1^- \int i_-^2 dt \, \tau_1}{q^- \int i_- dt}}$$

$$\approx 1 + \frac{\tau_1 N_1^+}{(1 - D_1^-) q_+} \left[\frac{\int i_-^2 dt}{\int i_- dt} - \frac{\int i_+^2 dt}{\int i_+ dt} \right] .$$

This assumes that $N_1^+/q_+ = N_1^-/q_-$. A similar equation holds for detector 2.

Since the beam current fluctuations during runs A and B are independent, we can approximate (1 - D) as:

$$1 - D \approx 1 + \sqrt{2}\ \frac{D_1 - D_2}{(1 - D)\ i}\ \left[\frac{\int i_-^2 dt}{q_-} - \frac{\int i_+^2 dt}{q_+}\right]$$

$$\equiv 1 + \sqrt{2}\ \frac{D_1 - D_2}{1 - D}\ d \quad .$$

A reasonable upper limit was calculated for d by determining what the effect would be of 120 hertz modulation on the beam current. For a sinusoidally-varying current, $i = i_0(1 + a \sin(\omega t))$, $d < 1/(120\pi\sqrt{n})$ for $a = 1$. ("a" for this experiment varied between one and zero.) "n"is the number of cycles of field reversal taken. This discussion assumes that the time duration of each cycle is not an integral multiple of the period of the 120 hertz modulation of the beam. This was the case for the present experiment since the time sequence generator was not locked in phase to the power line frequency. In 40 hours of running, corresponding to $\sigma(\delta) \approx 5 \times 10^{-5}$, $n = 9 \times 10^4$. Also $|D_1 - D_2| < 0.2$, and $D_1 \approx 0.5$ so $D < 1 \times 10^{-5}$. This gives an uncertainty in δ of $< 1 \times 10^{-6}$. This is negligible compared with the purely statistical error for the 40-hour period. It should be noted that this uncertainty decreases as $1/\sqrt{n}$ and thus remains negligible, since the statistical error decreases in the same way, as the duration of the experiment increases.

APPENDIX 3

The results presented in the following paper have recently been confirmed by Klepper and Spehl (1968).

Reprinted from

HYPERFINE STRUCTURE AND NUCLEAR RADIATIONS

Proceedings of a Conference Held at
Asilomar, Pacific Grove, California, U.S.A.
August 25 - 30, 1967

HYPERFINE FIELDS OF FLUORINE IN Ni AND Gd†

R. G. Stokstad, R. A. Moline, C. A. Barnes,
F. Boehm, and A. Winther

California Institute of Technology
Pasadena, California

1968

NORTH-HOLLAND PUBLISHING COMPANY - AMSTERDAM

Hyperfine Structure and Nuclear Radiations - North-Holland, Amsterdam (1968)

HYPERFINE FIELDS OF FLUORINE IN Ni AND Gd†

R. G. Stokstad, R. A. Moline, C. A. Barnes,
F. Boehm, and A. Winther

California Institute of Technology
Pasadena, California

The hyperfine magnetic fields at the sites of ^{19}F nuclei implanted in nickel and gadolinium have been measured. Pulsed beams of ^{4}He and also ^{19}F were used to observe the time-differential precession of the 0.197 MeV, $J^{\pi} = 5/2^{+}$ level of ^{19}F. Two hyperfields were observed in nickel at 300°K with values

$$H_{hf}^{1} = +17.8 \pm 0.4 \text{ kG},$$

$$H_{hf}^{2} = +90.2 \pm 1.4 \text{ kG}.$$

The value for the hyperfine field for ^{19}F in gadolinium at 103°K was found to be

$$H_{hf} = +12.9 \pm 0.4 \text{ kG}.$$

That the observed anisotropy of the time-differential γ-ray angular distribution in nickel is only about half that of the unperturbed distribution suggests that additional fields might be present to which these measurements were not sensitive.

Values for the mean life and g-factor of the 0.197-MeV level were found to be 128.7 ± 1.8 nanoseconds and 1.44 ± 0.04, respectively.

I. Introduction

The magnetic fields at the site of ^{19}F nuclei implanted in ferromagnetic crystal lattices have been studied in the course of an investigation of the low-lying levels of ^{19}F currently in progress at the California Institute of Technology. These magnetic fields have been measured by observing the time-differential rotation of the spin of the 0.197-MeV, $J^{\pi} = 5/2^{+}$ excited state of ^{19}F. The relatively long lifetime and precisely known[1] g-factor of this state make it particularly suitable for investigating fields from several kilogauss to as high as approximately 125 kilogauss, depending upon the minimum coincidence resolving time attainable. There is also a variety of methods by which the magnetic sublevels of the 0.197-MeV state may be unequally populated and which can therefore produce large anisotropies in the unperturbed γ-ray angular distribution of the 0.197-MeV deexcitation radiation.

For a magnetic field H perpendicular to the plane defined by the axis of nuclear alignment and direction of the deexcitation γ ray, the time-dependent angular distribution of the gamma radiation is given by

$$W(\theta, t) = 1 + B_2 \cos(2\theta + 2\omega_L t) + B_4 \cos(4\theta + 4\omega_L t), \quad (1)$$

where θ represents the angle between the nuclear alignment and the direction of the γ ray in the absence of a magnetic field, ω_L is the Larmor frequency of the spin rotation defined by

$$\hbar \omega_L = - g \mu_N H, \quad (2)$$

and B_2, B_4 are the coefficients of the unperturbed angular distribution. The elapsed time between formation and decay of the state is given by t, g is the gyromagnetic ratio of the state, and μ_N represents the nuclear magneton.

The axis of nuclear alignment and time of formation of the state are defined by a pulsed beam of particles incident on a target with the magnetic field H perpendicular to the plane containing the beam and the NaI γ-ray detector. Measurements have been made with a pulsed beam of 4.10-MeV ^{4}He particles bombarding a thin target of CaF_2 evaporated on various backings--nickel, gadolinium, and copper--and also with a pulsed beam of 30-MeV ^{19}F ions incident on clean foils of copper and nickel.

The analysis and results of these measurements, together with a more detailed description of the experimental arrangement, are presented in the following text.

II. Experimental Arrangement

The ONR-CIT tandem accelerator and associated neutron time-of-flight apparatus[2] were used to produce $^4He^+$ beam pulses with a time duration of about 2 nsec and average currents at the target of 0.1 μA. The system was designed for producing pulsed proton and ^{4}He beams, with the result that the bunching efficiency and hence average current of ^{19}F beams with a similar pulse duration were much smaller. The average current for a 30-MeV $^{19}F^{5+}$ beam of 2 nsec pulse duration was about 15 nA.

The γ rays were detected in a 1.27-cm-thick by 3.8-cm-diameter NaI(Tl) crystal coupled directly to an RCA 8575 photomultiplier. The face of the NaI(Tl) crystal was placed about 6 cm from the target for the time-differential measurements. A time-to-amplitude converter (TAC) was started by pulses from the anode of the photomultiplier and stopped by a 3.5-MHz signal from the beam-pulsing deflection plates. The output of the TAC was processed by a 400-channel pulse-height analyzer gated by a requirement that the γ-ray pulse height lie in the photopeak region of the 0.197-MeV transition. The time scale of the TAC was determined with a delay cable calibrated to an accuracy within 0.3%.

The external magnetic field used to align the domains of the ferromagnetic lattices was provided in some cases by an electromagnet

capable of producing a 9-kG field across a 1-cm gap. In other cases (notably the measurement on gadolinium) a small electromagnet was used, with the target foil clamped in its pole faces. The photomultiplier was suitably shielded from the stray fields associated with these magnets. The magnitude of the field H_{ext} produced by the electromagnet was measured with a Hall probe. Since the Hall probe is also sensitive to the direction of the magnetic field, it was used in conjunction with a reference magnet as a constant control in the measurements in which the sign of the external field was reversed.

The nickel and copper foils used in these experiments were of high purity (99.99%) and were annealed after having been rolled to thicknesses of 0.20 to 0.25 mm. The target foils were kept at room temperature when under bombardment by a flow of air directed at the back of the target. The sample of gadolinium from which a thin foil was fabricated was quoted to have a purity of greater than 99%. The foil was not annealed, and was maintained at a temperature of -170°C during the measurement.

III. Procedure

The ^{4}He bombarding energy of 4.10 MeV was determined by measuring an excitation function for the reaction $^{19}F(^4He, ^4He)^{19}F^*$ (0.197) over the energy range 4.0 to 4.3 MeV. There is a high density of narrow resonances[3] in the region of excitation of the ^{23}Na compound nucleus system populated by 3- to 5-MeV ^{4}He. It was therefore important to use a thin CaF_2 target ($\approx 25\ \mu g/cm^2$) and choose the incident ^{4}He energy carefully.

The unperturbed angular distribution of the 0.197-MeV radiation was determined by measuring the γ-ray yield as a function of angle for a direct-current beam incident on a copper-backed CaF_2 target mounted at 90 deg to the beam and with $H_{ext} \approx 0$. The NaI detector was positioned 240 mm from the target; it was estimated that the beam spot and center of rotation of the counter coincided to within 0.3 mm. After corrections for the finite solid angle subtended by NaI detector and for the γ-ray attenuation in the target backing, values of $B_2 = 0.16 \pm 0.02$ and $B_4 = 0.126 \pm 0.007$ were obtained. These values represent only lower limits on the anisotropy of the unperturbed angular distribution, since a small electric quadrupole attenuation in the copper backing cannot be excluded.

The copper backing was then placed in an 8.7-kG external magnetic field, and the time-differential precession of the unperturbed angular distribution was observed for opposing directions of the applied field, by using the pulsed beam. The NaI counter was fixed at 45 deg and at a distance of 60 mm from the target. Following the procedure described in Section IV, an analysis of the time-differential spectrum yielded values of $B_2 = 0.184 \pm 0.002$ and $B_4 = 0.109 \pm 0.003$. These values are thus in good agreement with those measured using a direct-current beam and movable γ-ray detector.

The measurements on nickel were done in exactly the same manner as described above for copper. The measurement on gadolinium was

slightly different in that the gadolinium foil was tilted at an angle of 45 deg with respect to the beam and clamped in the pole faces of a small electromagnet inside the vacuum.

The experimental arrangements for the cases in which a ^{19}F beam was used were the same as those described above. No measurement of the unperturbed γ-ray angular distribution using a direct-current beam was attempted. A large number of the incident fluorine ions are scattered at angles greater than 90 deg and hence can leave the target and decay in the walls of the target chamber, since the distance traveled by a 30-MeV ^{19}F ion within the mean lifetime of the 0.197-MeV state is about 1.7 meters. A time-differential measurement in copper of the unperturbed angular distribution, however, yielded a value of $B_2 = 0.036$. This is about one-half as large as the value predicted by Coulomb excitation theory[4] under the (invalid) assumption that all the ^{19}F projectiles are stopped in the target. The value of B_4 is expected to be about one-eighth of B_2 according to Coulomb excitation theory. The use of the ^{19}F beam thus has the disadvantage that much smaller anisotropies are obtained than with the ^4He beam.

As noted earlier, the magnitude and direction of the magnetic field were determined with a Hall probe. In order to eliminate any uncertainties due to hysteresis in the electromagnet and in the ferromagnetic samples, the current in the electromagnet was always first raised to a large value and then lowered to the value producing the desired external magnetic field.

IV. Analysis

The time-differential measurements were analyzed in the following manner. The time spectrum from the multichannel analyzer was divided by an exponential with a mean decay time of 128 nsec. Whenever necessary, a slight normalization of either of the two spectra corresponding to field "up" or field "down" was made in order that, after subtraction of the two spectra, the resulting time spectrum would contain oscillations centering about zero. The reason for dividing the individual spectra by an analytical exponential rather than by the sum of the two spectra was to avoid the introduction of oscillations of the form $\cos(4\omega_L t)$, the latter being contained in the summed spectra. The difference of the two spectra for field up and field down with the NaI detector at 45 deg to the beam contains only terms in $\sin(2\omega_L t)$. After suitable normalization, the resulting spectrum is given by

$$\begin{aligned} A(t) &= \tfrac{1}{2}[W(\theta - \omega_L t) - W(\theta + \omega_L t)] \\ &= B_2 \sin(2\omega_L t)\sin(2\theta) + B_4 \sin(4\omega_L t)\sin(4\theta) \\ &= B_2 \sin(2\omega_L t), \quad \text{for } \theta = 45 \text{ deg.} \end{aligned} \tag{3}$$

The reduced data A(t) were analyzed by different though nearly equivalent methods. A straightforward Fourier analysis of A(t) with the Fourier coefficients given by

$$A(\omega) = \frac{2}{t_2 - t_1} \sum_{t=t_1}^{t_2} A(t) \cos \omega t,$$

$$B(\omega) = \frac{2}{t_2 - t_1} \sum_{t=t_1}^{t_2} A(t) \sin \omega t \qquad (4)$$

yielded essentially the same results regardless of whether or not ω was constrained by the requirement $\omega(t_2 - t_1) = 2\pi n$, where n is an integer. This is a consequence of the fact that

$$\frac{1}{t_2 - t_1} \sum_{t=t_1}^{t_2} A(t) \approx 0 . \qquad (5)$$

Some of the data were also analyzed by the method of least squares. In this method the frequency ω was given and the amplitude and phase of the oscillations, $A \cos \omega t + B \sin \omega t$, were fitted to the data. The value of χ^2 as a function of ω then indicated the presence of any oscillations in the data. This technique, whereby only one frequency is considered, is algebraically identical to the Fourier analysis, but with $A(t)$ replaced by $A(t)/[\Delta A(t)]^2$. These two methods of analysis therefore gave nearly identical results. Where the Fourier analysis method showed an indication of more than one frequency of oscillation present in the data, the least-squares method was used with several values of ω given simultaneously. The change in χ^2 with the inclusion of more than one frequency in the fitting procedure then provided an additional test of the presence of several frequencies.

Since the data cover only a finite interval of time, a Fourier analysis of a pure sinusoidal oscillation yields not one but many peaks in the spectrum of the Fourier transform. The dominant peak corresponds to the pure sine wave, and the sizes of the smaller subsidiary peaks depend, of course, on the number of oscillations contained in the interval subjected to the analysis. The presence of these subsidiary peaks greatly complicates the analysis of the data with regard to the presence of oscillations with amplitudes substantially smaller than those of the main oscillation. A Fourier analysis of data from which the main oscillation has been subtracted can provide some additional information on the presence of oscillations of small amplitude and also on the nature of the distribution, if any, of frequencies within the main oscillation. This question of additional oscillations in the time-differential spectra is important, since in none of the cases reported here is the full anisotropy of the unperturbed angular distribution accounted for by the amplitudes of the main oscillations observed in the measurements on ferromagnetic lattices.

The total magnetic field at the site of the nucleus is denoted by H and is related to the measured quantity ω_L by Eq. (2). It is convenient

to remove those contributions to H which depend upon the external field and shape of the sample. Thus

$$H \equiv H_{ext} - DM + H_{hf} \ , \tag{6}$$

where H_{ext} represents the external field, M is the magnetization of the sample, and D is the demagnetization factor. It is noted that the hyperfine field H_{hf} as defined by the above equation includes the Lorentz field. Since it is a good approximation to neglect the demagnetization factor for a thin foil with the magnetization in the plane of the foil, we have

$$H_{hf} = H - H_{ext}. \tag{7}$$

V. Results

A measurement of the mean lifetime of the 0.197-MeV state in ^{19}F, using a ^{19}F beam and a copper target in the absence of an external field, yielded a value of 128.7 ± 1.8 nsec, in agreement with the 129.9 ± 2.3 nsec obtained by Becker, Olness, and Wilkinson. [5]

The time-differential spectrum A(t) for ^{19}F recoiled from ^{4}He into a copper backing in an external field of 8.7 kG is shown in Fig. 1. The full curve is a least-squares fit to the data over the region shown. The value of the g-factor obtained from this measurement is 1.44 ± 0.04, which agrees with 1.436 ± 0.007 from the work of Schmidt et al. [1] The latter value has been used in the work presented here.

Figures 2 and 3 show the data from similar measurements using a nickel target backing in external fields of 8.8 and 0.32 kG, respectively. A comparison of Figs. 2 and 3 with Fig. 1 shows immediately that

(a) the sign of the hyperfine field in nickel is positive, i. e., parallel to the magnetization;

(b) the amplitude of the oscillations in the nickel data is significantly smaller than in copper;

(c) there are at least two frequency components in the nickel spectra, and hence at least two hyperfine fields in nickel; this is clearly demonstrated by the Fourier transform of the data shown in Fig. 4.

It should be noted that there are three frequencies indicated in the data shown in Fig. 2. The lowest frequency component is due to the small portion (about 6%) of ^{19}F nuclei which have remained in the CaF_2 target and hence decay in the external field of 8.8 kG.

The results of least-squares analyses of the data are listed in Table I. The period and amplitude of the oscillation fitted to the reduced data A(t) together with the associated value of χ^2/N are given in the last three columns. N is the number of degrees of freedom minus 1, and ranged from values of 150 to 200. The brackets indicate where several frequencies were simultaneously included in the least-squares method. The improvement in χ^2 upon the addition of a second frequency in nickel with a period of about 5 nsec is very marked. This frequency occurred consistently in the data obtained in experiments using both ^{4}He and ^{19}F beams as well as for all values of H_{ext}.

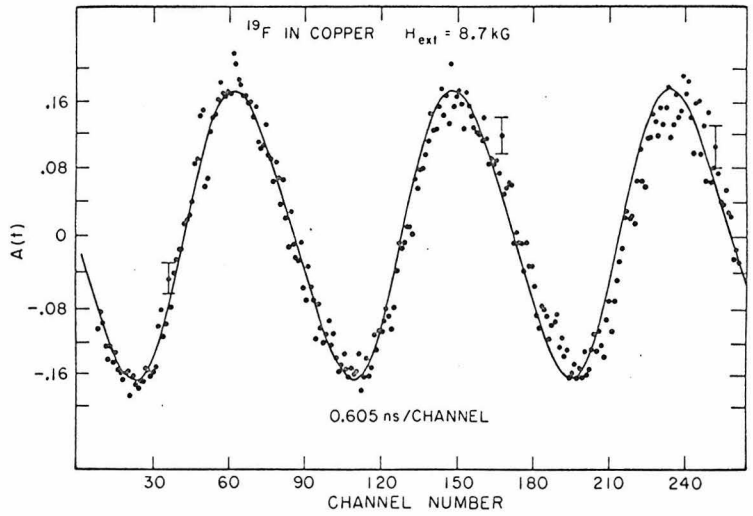

Fig. 1. The time differential precession of the 0.197-MeV $J^{\pi} = 5/2^{+}$ level in ^{19}F recoiled from ^{4}He in an external magnetic field of 8.7 kG. The solid curve is a least-squares fit to the data.

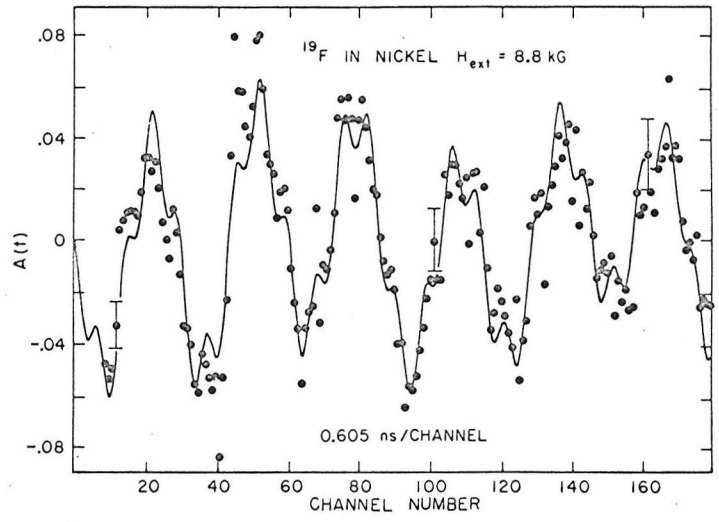

Fig. 2. Similar to Fig. 1 but with the copper target backing replaced by nickel. The amplitude of the oscillation is smaller than that in Fig. 1.

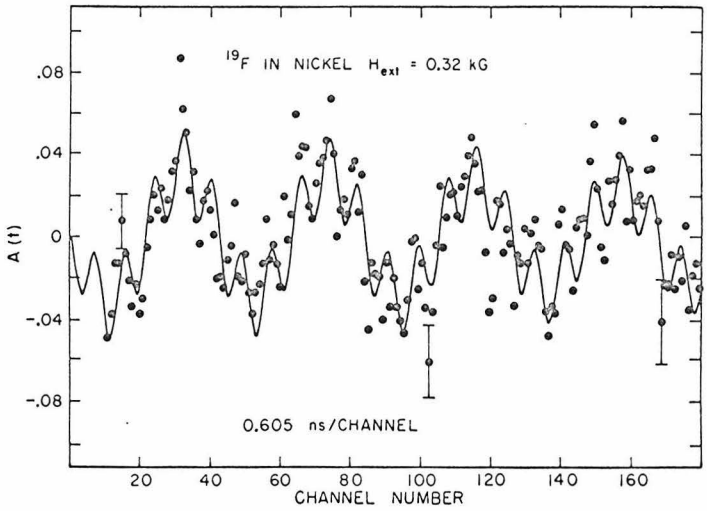

Fig. 3. Similar to Fig. 2 but with the external field reduced to 0.3 kG.

Figure 5 shows the results of the measurements on nickel with a ^{4}He beam for various values of H_{ext}. The values of the two hyperfine fields in nickel at 300°K as defined by Eq. (7) are

$$H_{hf}^1 = +17.8 \pm 0.4 \text{ kG},$$

$$H_{hf}^2 = +90.2 \pm 1.4 \text{ kG}.$$

The slope of both lines in Fig. 5 is $\Delta H/\Delta H_{ext} = 0.975 \pm 0.035$, which is consistent with the assumption of a negligible demagnetization factor for the thin-foil samples.

From an inspection of the Fourier transform of the data from which the two known frequencies have been subtracted, it appears that any other oscillations corresponding to additional hyperfine fields in nickel of less than 100 kG must have amplitudes less than one-fourth of the amplitude corresponding to H_{hf}^1.

It may be noted from Table I that a second period at twice the fundamental frequency appears in the data for the measurement on copper with H_{ext} = 8.7 kG. This is because the effective angle of the γ-ray detector differed slightly from 45 deg. From Eq. (3) it is seen that $\theta \neq 45$ deg introduces a term containing $B_4 \sin(4\omega_L t)$. Since the amplitude of this term is smaller than the fundamental frequency by a factor of 10, it was neglected in the analyses of the measurements on nickel and gadolinium.

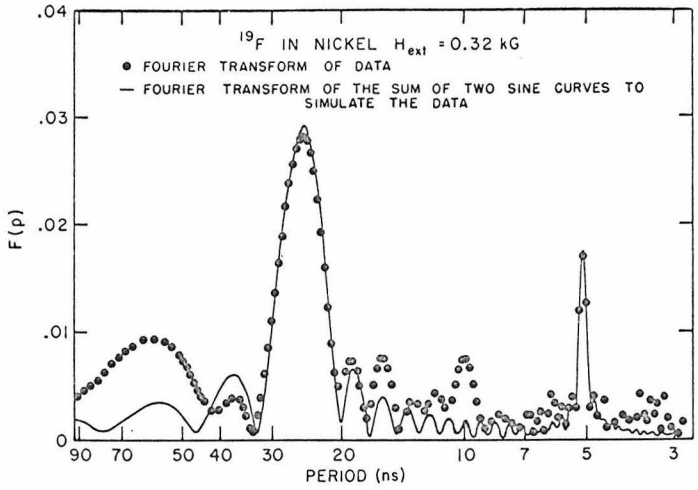

Fig. 4. The solid circles are the transform, F(p, of the data shown in Fig. 3.

$$F(p) = \sqrt{A^2(\omega) + B^2(\omega)},$$

where $p = 2\pi/\omega$, and $A(\omega)$ and $B(\omega)$ are cosine and sine transforms of the data, as defined by Eq. (4). The solid curve is the transform of the sum of two sine curves that simulate the data.

For the peaks at 25 and 5 nsec the amplitude, $A(\omega)$, of the cosine transform was zero. Thus, the experimental data can be fitted by a pure sine transform, in agreement with Eq. (3).

Note the subsiding maxima caused by the finite time length of the data sample, as discussed in Section II of the text.

The sum of the amplitudes of the oscillations corresponding to H_{hf}^1, H_{hf}^2, and the small number of ^{19}F nuclei precessing in the external field is about one-half that of the amplitude of the oscillation observed in the measurements with a copper backing, even after correcting for the 2.5-nsec time resolution of the experiment. (The period of oscillation of H_{hf}^2 is about 5 nsec, which results in a 40 to 60% attenuation, assuming a square or Gaussian time-resolution function, respectively.) It must be concluded, therefore, that approximately 50% of the ^{19}F nuclei implanted in nickel by the recoil method must be precessing in hyperfine fields which are not detected by these measurements. Some of the ^{19}F recoils may be precessing in fields higher than about 100 kG, in which case $2\omega_L$ would be too large to detect with the present time resolution. In addition, the precession frequencies could also be distributed more or less continuously over the range of the present experiment without any frequency component having an

Table I. The results of a least-squares analysis of measurements using beams of ^4He and ^{19}F for various values of H_{ext}. Columns 1–3 give the target and backing, the beam, and the value of the external field. Columns 4 and 5 give the period and amplitude of the sinusoidal oscillation in the reduced data, A(t), while column 6 gives the accompanying value of χ^2 divided by the number of degrees of freedom minus 1. The brackets indicate where the presence of more than one oscillation has been included in the least-squares analysis. The improvement in χ^2/N upon the inclusion of a second oscillation in the nickel data with a period of approximately 5 nsec is noted.

Experiment			Analysis		
Target	Beam	H_{ext} (kG)	Period (nsec)	Amplitude	χ^2/N
CaF_2-Cu	^4He	0	∞	0	0.80
CaF_2-Cu	^4He	8.7	52.3	0.171	1.88
			52.3 26.1	0.171 0.015 }	1.49
CaF_2-Ni	^4He	8.8	17.3	0.042	3.8
			17.3 4.63	0.042 0.012 }	3.0
			17.3 4.63 51.7	0.042 0.012 } 0.013	2.2
CaF_2-Ni	^4He	1.3	24.0	0.035	2.34
			24.0 4.99	0.035 0.018 }	1.47
CaF_2-Ni	^4He	0.32	25.1	0.029	2.13
			25.1 5.05	0.029 0.017 }	1.36
Ni	^{19}F	0.48	∞	0	1.26
			24.5	0.0097	1.04
			24.5 4.91	0.0097 0.0073 }	0.90
CaF_2-Gd	^4He	0.59	33.9	0.0141	1.28

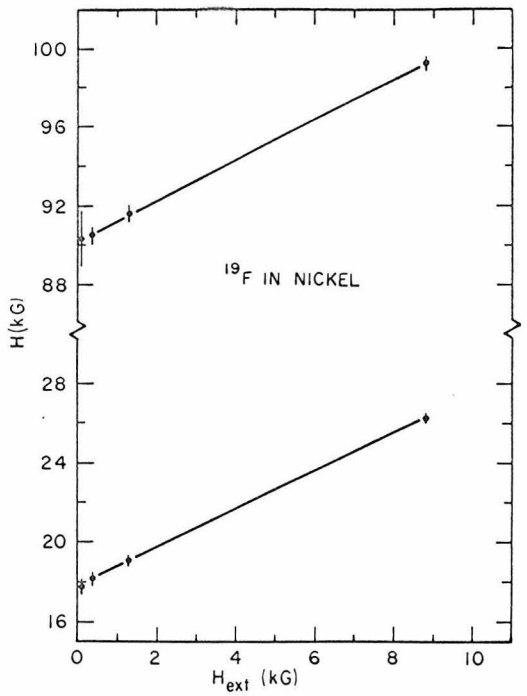

Fig. 5. The dependence of the total magnetic field H, at the site of the ^{19}F nucleus in nickel, on the external field H_{ext}.

amplitude greater than approximately one-fourth that of the frequency corresponding to H_{hf}^1.

There is a consistent decrease in the amplitude of the oscillation corresponding to H_{hf}^1 in nickel as the value of H_{ext} is decreased. At the same time, however, it appears that the amplitude corresponding to H_{hf}^2 increases. At least part of this increase may be due to the increase of the Larmor period as H_{ext} is decreased. A measurement with H_{ext} = 0.03 kG yielded very small amplitudes for the oscillations corresponding to H_{hf}^1 and H_{hf}^2. This latter effect is due to the partial disalignment of the magnetic domains in a very weak external field.

Figure 6 shows the results of the measurement on gadolinium at -170°C. The hyperfine field is

$$H_{hf} = 12.9 \pm 0.4 \text{ kG}.$$

It is not possible to draw any quantitative conclusion about the very small amplitude of the oscillation in the reduced time spectrum for gadolinium. This is because the gadolinium foil was at an angle of

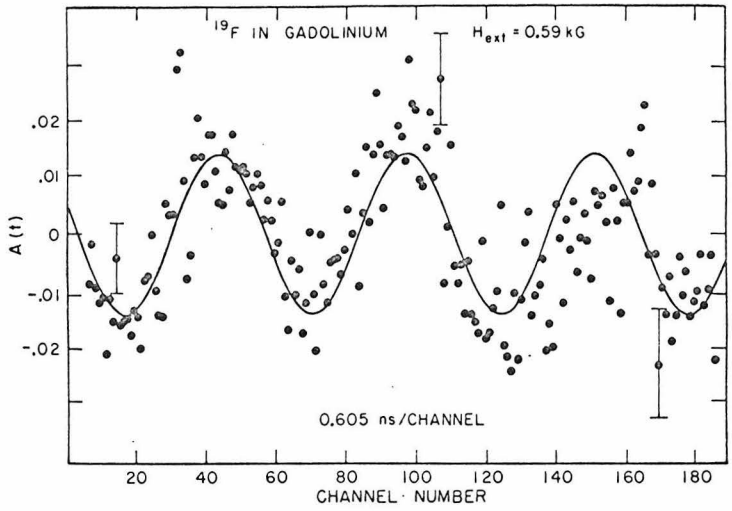

Fig. 6. The time-differential precession of the 0.197-MeV level in ^{19}F in gadolinium in an external magnetic field of 0.59 kG. The solid curve is a least-squares fit to the data.

45 deg to the beam, and therefore the unperturbed γ-ray angular distribution measured with a copper target backing at 90 deg to the beam may not be correct here. It appears unlikely, however, that the amplitude of the oscillation observed in this measurement corresponds to the full amplitude of the unperturbed angular distribution.

Similar investigations with an iron host are in progress. A preliminary value of H_{hf} for ^{19}F in Fe at 300°K is 92 kG.

Measurements similar to those presented here have recently been reported for ^{19}F in iron, cobalt, and nickel by Braunsfurth et al.[6] A comparison of their work on nickel with the results reported here shows fair agreement on the magnitude of H_{hf} at 300°K. There is disagreement, however, on the sign of the hyperfine field for external fields below 1 kG. The hyperfine field at 90 kG was not reported by Braunsfurth et al., but they report two satellite fields not observed in the present work, one of which may possibly have been below the level of detectability here.

The authors wish to thank T. Lauritsen for his interest in this work. They wish also to thank H. J. Körner for kindly communicating results prior to publication. The assistance of E. Adelberger and H. Henrikson is gratefully acknowledged.

Footnote and References

†Work done in part under auspices of the Office of Naval Research [Nonr-220(47)] and the U. S. Atomic Energy Commission [AT(04-3)-63].

1. H. Schmidt et al., Phys. Letters 24B, 457 (1967).
2. E. Adelberger, Nucl. Instr. Methods 47, 327 (1967).
3. R. M. Freeman and G. S. Mani, Nucl. Phys. 51, 593 (1964).
4. K. Alder et al., Rev. Mod. Phys. 28, 432 (1956).
5. J. A. Becker, J. W. Olness, and D. H. Wilkinson, Phys. Rev. 155, 1089 (1967).
6. J. Braunsfurth, J. Morgenstern, H. Schmidt, and H. J. Körner, Z. Physik 202, 321 (1967).

Discussion

E. Matthias: In one of your figures, you had only a polarizing field of 320 gauss. This small field may have introduced a second frequency component due to incomplete polarization. Secondly, one should measure the high-frequency component by NMR methods. The 90-kG hyperfine field should be sufficient to do this experiment.

H. J. Körner: In similar measurements at Hamburg we observed satellite fields of 15 kG and 11 kG which were especially pronounced at 77°K. The amplitude of this component amounts to about 15%. These measurements were very recently repeated with 99.999% pure nickel foil and better statistics than shown today. We get essentially the same results as presented here, and we definitively observe the high-field component. Contrary to our old measurements, the amplitudes of the low-field satellite components were found to be reduced appreciably. This leads us to believe that the low field may be due to impurities in the nickel foil.

N. J. Stone (question to Dr. Körner): Might the low-frequency component be correlated to interstitials which are more stable at low temperatures?

H. J. Körner: That is exactly the explanation which we gave.

REFERENCES

Abov, Yu.G., Krupchitsky, P.A., Bulgakov, M.I., Yermakov, O.N. and Karpikhin, I.L., Physics Letters 27B, 16 (1968).

Alder, K., Bohr, A., Huus, T., Mottelson, B., and Winther, A., Rev. Mod. Phys. 28, 432 (1956a).

Alder, K. and Winther, A., Mat. Fys. Medd. Dan. Vid. Selsk. 31 (1956b).

Alexander, T.K., Allen, K.W., and Healey, D.C., Physics Letters 20, 402 (1966).

Boehm, F. and Kankeleit, E., Nuclear Phys. A109, 457 (1968).

Bougnot, G., Espi, G., Poizat, J.C., Samueli, J.J., and Sarazin, A., Journal de Physique 26, 546 (1965).

Chesler, R.B., Nuclear Inst. and Methods 37, 185 (1965).

Feynman, R.P. and Gell-Mann, M., Phys. Rev. 109, 193 (1958).

Gale, N.H. and Calvert, J.M., Physics Letters 7, 348 (1963).

Klepper, O. and Spehl, H., to be published (1968).

Lauritsen, T. and Ajzenberg-Selove, F., Energy Levels of Light Nuclei, Nuclear Data Tables (1962).

Lobashov, V.M., Nazarenko, V.A., Saenko, L.F., Smotritskii, L.M., and Kharkevich, G.I., JETP Letters 3, 173 (1966) and 5, 59 (1967).

Maqueda, E., Physics Letters 23, 571 (1966).

McKellar, B.H.J., Phys. Rev. Letters 20, 1542 (1968).

Michel, F.C., Phys. Rev. 133, B329 (1964).

Olness, J.W. and Warburton, E.K., Phys. Rev. 156, 1145 (1967).

Paul, H., McKeown, M., and Scharff-Golkhaber, G., Phys. Rev. 158, 1112 (1967).

Schiott, H.E., "Projected Ranges of Light Ions in Heavy Substances", preprint Aarhus University (1967).

Segel, R.E., Olness, J.W., and Sprenkel, E.L., Phys. Rev. 123, 1382 (1961).

Shukla, A.P., private communication (1968).

Steffen, R.M. and Frauenfelder, H., Alpha-, Beta-, and Gamma-Ray Spectroscopy, edited by K. Siegbahn (North-Holland Pub. Co., Amsterdam), p. 1456 (1965).

Tanner, N., Phys. Rev. 107, 1203 (1957).

Whittaker, E.T. and Watson, G.N., A Course of Modern Analysis, Fourth Edition (The Syndics of the Cambridge University Press, New York), p. 343 (1963).

Wilkinson, D.H., Phys. Rev. 109, 1603 (1958).

Winther, A., private communication (1967).